Chemically-Generated Stationary Inverted Lyman Population for a CW HI Laser

R. Mills, P. Ray, R. Mayo
BlackLight Power, Inc.
493 Old Trenton Road
Cranbury, NJ 08512

ABSTRACT

Each of the ionization of Rb^+ and cesium and an electron transfer between two K^+ ions (K^+ / K^+) provide a reaction with a net enthalpy of an integer multiple of the potential energy of atomic hydrogen, 27.2 eV. The corresponding Group I nitrates provide these reactants as volatilized ions directly or as atoms by undergoing decomposition or reduction to the corresponding metal. The presence of each of the reactants identified as providing an enthalpy of 27.2 eV formed a low applied temperature, extremely low voltage plasma called a resonance transfer or rt-plasma having strong vacuum ultraviolet (VUV) emission. In contrast, magnesium and aluminum atoms or ions do not ionize at integer multiples of the potential energy of atomic hydrogen. $Mg(NO_3)_2$ or $Al(NO_3)_3$ did not form a plasma and caused no emission.

For further characterization, we recorded the width of the 6563 Å Balmer α line on light emitted from rt-plasmas. Significant line broadening of 18, 12, *and* 12 eV was observed from a rt-plasma of hydrogen with KNO_3, $RbNO_3$, and $CsNO_3$, respectively, compared to 3 eV from a hydrogen microwave plasma. These results could not be explained by Stark or thermal broadening or electric field acceleration of charged species since the measured field of the incandescent heater was extremely weak, 1 V/cm, corresponding to a broadening of much less than 1 eV. Rather the source of the excessive line broadening is consistent with that of the observed VUV emission, an energetic reaction caused by a resonance energy transfer between hydrogen atoms and K^+ / K^+, Rb^+, and cesium, which serve as catalysts.

KNO_3 and $RbNO_3$ formed the most intense plasma. Remarkably, a stationary inverted Lyman population was observed in the case of an rt-plasma formed with potassium and rubidium catalysts. These catalytic reactions may pump a cw HI laser as predicted by a collisional radiative model used to determined that the observed overpopulation was above threshold.

1. Introduction

The Lyman α, β, and γ lines of atomic hydrogen at $121.6\,nm$, $102.6\,nm$, and $97.3\,nm$ in the vacuum ultraviolet (VUV) region are due to the transitions from $n=2$, $n=3$, and $n=4$ to $n=1$, respectively. These lines are of great importance in many applications ranging from photochemistry, to laboratory simulations of planetary atmospheres, to astrophysics and plasma physics. In plasma physics, the Lyman series line intensities and their ratios are frequently used in the determination of plasma parameters such as hydrogen number densities and other quantities such as particle fluxes or ion recombination processes [1-2]. For the last four decades, scientist from academia and industry have been searching for lasers using hydrogen plasma [3-6]. Developed sources that provide a usefully intense hydrogen plasma are high powered lasers, arcs and high voltage DC and RF discharges, synchrotron devices, inductively coupled plasma generators, and magnetically confined plasmas. However, the generation of population inversion is very difficult. Recombining expanding plasmas jets formed by methods such as arcs or pulsed discharges is considered one of the most promising methods of realizing an HI laser.

It was reported previously that a new plasma source has been developed that operates by incandescently heating a hydrogen dissociator to provide atomic hydrogen and heats a catalyst such that it becomes gaseous and reacts with the atomic hydrogen to produce a plasma called a resonance transfer or rt-plasma. It was extraordinary, that intense VUV emission was observed by Mills et al. [7-8] at low temperatures (e.g. $\approx 10^3\,K$) and an extraordinary low field strength of about 1-2 V/cm from atomic hydrogen and certain atomized elements or certain gaseous ions which singly or multiply ionize at integer multiples of the potential energy of atomic hydrogen, $27.2\,eV$. The theory was given previously [9-11].

The Group I and Group VIII elements are unique in that, with the exception of xenon, atoms and or ions from these groups provide a reaction with a net enthalpy that is a close match to an integer multiple of the potential energy of atomic hydrogen, $m \cdot 27.2\,eV$ where m is an integer. The corresponding reactions of Group I elements with a net

enthalpy of $m \cdot 27.2\,eV$ which are proposed to form an rt-plasma follow:

The first and second ionization energies of lithium are $5.39172\,eV$ and $75.6402\,eV$, respectively [12]. The double ionization reaction of Li to Li^{2+}, then, has a net enthalpy of reaction of $81.032\,eV$, which is equivalent to $m = 3$.

The second, third, and fourth ionization energies of sodium are $47.2864\,eV$, $71.6200\,eV$, and $98.91\,eV$, respectively [12]. The triple ionization reaction of Na^+ to Na^{4+}, then, has a net enthalpy of reaction of $217.8164\,eV$, which is equivalent to $m = 8$.

The second ionization energy of potassium is $31.63\,eV$, and K^+ releases $4.34\,eV$ when it is reduced to K [12]. The combination of reactions K^+ to K^{2+} and K^+ to K, then, has a net enthalpy of reaction of $27.28\,eV$, which is equivalent to $m = 1$. Also, the first, second, and third ionization energies of potassium are $4.34066\,eV$, $31.63\,eV$, and $45.806\,eV$, respectively [12]. The triple ionization reaction of K to K^{3+}, then, has a net enthalpy of reaction of $81.7766\,eV$, which is equivalent to $m = 3$.

The second ionization energy of rubidium is $27.28\,eV$ [12]; thus, the reaction Rb^+ to Rb^{2+} has a net enthalpy of reaction of $27.28\,eV$, which is equivalent to $m = 1$.

The first and second ionization energies of cesium are $3.89390\,eV$ and $23.15745\,eV$, respectively [12]. The double ionization reaction of Cs to Cs^{2+}, then, has a net enthalpy of reaction of $27.05135\,eV$, which is equivalent to $m = 1$.

Rt-plasmas with Group I catalysts were reported previously [7]. In this paper, we report on further characterization of rt-plasmas with Group I catalysts wherein $m = 1$. Group I nitrates were used since they are volatile at relatively low temperatures and also undergo hydrogen reduction and gradual thermal decomposition. Thus, they provide gaseous ions M^+ or atoms M.

The energetic hydrogen atom densities and energies were calculated from the width of the 6563 Å Balmer α line emitted from a control hydrogen microwave plasma and rt-plasmas. The characteristic emission from the catalyst was measured. KNO_3 and $RbNO_3$ formed the most intense plasmas. Remarkably, the population of the levels $n = 3$ and $n = 4$ of hydrogen were continuously inverted with respect to $n = 2$ in an rt-plasma formed with the K^+ and Rb^+ catalysts. To our knowledge, this

is the first report of population inversion in a chemically generated plasma. The plasma was further characterized by measuring the electron temperature T_e from intensity ratios of alkali lines.

2. Experimental

The VUV spectrum (900 – 1300 Å), the width of the 6563 Å Balmer α line, and the high resolution visible spectrum were recorded on light emitted from a hydrogen microwave discharge performed according to methods reported previously [13-14] that served as a control for measurements recorded on light emitted from rt-plasmas of hydrogen with KNO_3, $RbNO_3$, or $CsNO_3$. The experimental set up described previously [7-8] and shown in Figure 1 comprised a thermally insulated quartz cell with a cap that incorporated ports for gas inlet, outlet, and photon detection. A tungsten filament heater and hydrogen dissociator were in the quartz tube as well as a cylindrical titanium screen that served as a second hydrogen dissociator that was coated with catalysts KNO_3, $RbNO_3$, or $CsNO_3$ and control materials $Mg(NO_3)_2$ or $Al(NO_3)_3$. The cell was maintained at 50 °C for four hours with helium flowing at 30 sccm at a pressure of 0.1 Torr. The cell was then operated with and without an ultrapure hydrogen flow rate of 5.5 sccm maintained at 300 mTorr. The titanium screen was electrically floated with 250 W of power applied to the filament. The temperature of the tungsten filament was estimated to be in the range 1100 to 1500 °C. The external cell wall temperature was about 700 °C.

The rt-plasma phenomena was also studied for cesium metal with hydrogen versus additional controls. The quartz cell was operated under the same conditions as for the Group I nitrates with 1.) hydrogen, argon, neon, and helium alone; 2.) sodium, magnesium, barium, and cesium metals alone, and 3.) sodium, magnesium, barium, and cesium with hydrogen. The pure elements of sodium, magnesium, barium, and cesium were placed in the bottom of the cell and vaporized by filament heating.

The VUV spectrometer was a normal incidence 0.2 meter monochromator equipped with a 1200 lines/mm holographic grating with a platinum coating that covered the region 20 – 5600 Å. The VUV spectrum was recorded with a CEM. The wavelength resolution was

about 0.2 Å (FWHM) with slit widths of 50 μm. The increment was 2 Å and the dwell time was 500 ms. The VUV spectrum (900 – 1300 Å) of the rt-plasma cell emission was recorded at about the point of the maximum Lyman α emission to confirm the rt-plasma before the line broadening and high resolution visible spectrum in the region of 4070 Å were recorded.

In addition, regions of the VUV, ultraviolet (UV) and visible (VIS) spectra (400 – 5600 Å) were recorded with the normal incidence VUV spectrometer using a PMT and a sodium salicylate scintillator to record emission from the atoms and ions of rt-plasma catalysts. The emission was compared with a standard VUV emission spectrum of potassium that was obtained with a gas discharge cell comprised a five-way stainless steel cross that served as the anode with a hollow stainless steel cathode that was coated with KNO_3, $RbNO_3$, or $CsNO_3$ by the same procedure used to coat the titanium dissociator. The five-way cross was pressurized with 1 torr of hydrogen to initiate the discharge. The hydrogen was then evacuated so that only catalyst lines were observed. The DC voltage at the time the spectra were recorded was 300 V.

The electron temperatures T_e of the $RbNO_3$ and KNO_3 cells were measured from the ratio of the intensity of the Rb^+ 741.4 Å line to that of the Rb^{2+} 815.3 Å line and the ratio of the K^+ 612.6 Å line to that of the K^{2+} 546.1 Å line, respectively, as described by Griem [15].

The plasma emission from a hydrogen microwave discharge [14] control and each rt-plasma maintained in the filament heated cell was fiber-optically coupled to a high resolution visible spectrometer capable of a resolution of ±0.06 Å. The slits were set to 20 μm, the step size was 0.1 Å, and the spectra (4100.5 – 4103.5 Å, 4338.5 – 4343.5 Å, 4859.0 – 4864.0 Å, and 6560 – 6570 Å) were recorded by a PMT in a single accumulation with a 1 second integration time.

To measure the absolute intensity, the high resolution visible spectrometer and detection system were calibrated [16] with 5460.8 Å, 5799.6 Å, and 6965.4 Å light from a Hg-Ar lamp (Ocean Optics, model HG-1) that was calibrated with a NIST certified silicon photodiode. The population density of the n=3 hydrogen excited state N_3 was determined from the absolute intensity of the Balmer α (6562.8 Å) line measured using the calibrated spectrometer. The absolute intensities of Balmer β,

γ, and δ were determined from the absolute intensity of Balmer α and the relative intensity ratios.

The spectrometer was calibrated between 400-2000 Å with a standard discharge light source using He, Ne, Ar, Kr, and Xe lines: He I (584 Å), He II (304 Å), Ne I (735 Å), Ne II (460.7 Å), Ar I (1048 Å), Ar II (932 Å), Kr II (964 Å), Xe I (1295.6 Å), Xe II (1041.3 Å), Xe II (1100.43 Å). The wavelength and intensity ratios matched those given by NIST [17]. The spectrometer response was determined to be approximately flat in the 1000-1300 Å region. The calculation of the number density of the n=2, 3, and 4 states was corrected for the minor variation of the sensitivity with wavelength in this region.

3. Results and discussion

A. Measurement of hydrogen atom temperature and number density from Balmer line broadening

The method of Videnovic et al. [18] was used to calculate the energetic hydrogen atom densities and energies from the width of the 6563 Å Balmer α line emitted from microwave and rt-plasmas. The full half-width $\Delta\lambda_G$ of each Gaussian results from the Doppler ($\Delta\lambda_D$) and instrumental ($\Delta\lambda_I$) half-widths:

$$\Delta\lambda_G = \sqrt{\Delta\lambda_D^2 + \Delta\lambda_I^2} \tag{1}$$

$\Delta\lambda_I$ in our experiments was 0.06 Å. The temperature was calculated from the Doppler half-width using the formula:

$$\Delta\lambda_D = 7.16\, X\, 10^{-6}\lambda_0\left(\frac{T}{\mu}\right)^{1/2} \quad (\text{Å}) \tag{2}$$

where λ_0 is the line wavelength in Å, T is the temperature in K ($1\,eV = 11{,}605\,K$), and μ is the molecular weight (=1 for hydrogen). In each case, the average Doppler half-width that was not appreciably changed with pressure varied by ±5% corresponding to an error in the energy of ±5%. The corresponding number densities for noble gas-hydrogen mixtures varied by ±20% depending on the pressure.

The results of the 6563 Å Balmer α line width measured with the high resolution (±0.06 Å) visible spectrometer on light emitted from rt-plasmas of hydrogen with KNO_3, $RbNO_3$, and $CsNO_3$ are shown in Figures 2-

4, respectively. Significant line broadening of 18, 12, *and* 12 *eV* and atom densities of $4 X 10^{11}$, $6 X 10^{11}$, *and* $4 X 10^{11}$ *atoms/cm*^{3} were observed from a rt-plasma of hydrogen with KNO_3, $RbNO_3$, and $CsNO_3$, respectively, as shown in Table 1. A hydrogen microwave plasma maintained at the same total pressure showed no excessive broadening corresponding to an average hydrogen atom temperature of $\approx 3\,eV$ and a density of $2 X 10^{11}$ *atoms/cm*^{3}.

In addition to the Balmer α line, the Balmer β, γ, and δ lines corresponding to n=3, n=4, and n=5 were also broadened as shown for the case of the $RbNO_3$ rt-plasma emission in Figures 5-7, respectively. The line broadening results could not be explained by Stark or thermal broadening or electric field acceleration of charged species since the measured field of the incandescent heater was extremely weak, 1 V/cm, corresponding to a broadening of much less than 1 eV. We propose that the Doppler broadening was caused by the energetic reaction which formed the rt-plasma.

Prior studies that reported fast H attributed the observation to acceleration of ions in a high electric fields at the cathode fall region and an external field Stack effect [18-21]. The authors have reported observations with a microwave plasma having no high field present [14, 22]. Microwave helium-hydrogen and argon-hydrogen plasmas showed extraordinary broadening corresponding to an average hydrogen atom temperature of 110-130 *eV* and 180-210 *eV*, respectively. Whereas, pure hydrogen and xenon-hydrogen microwave plasmas showed no excessive broadening corresponding to an average hydrogen atom temperature of $\approx 4\,eV$ [14].

No hydrogen species, H^+, H_2^+, H_3^+, H^-, H, or H_2, responds to the microwave field; rather, only the electrons respond. But, the measured electron temperature in the argon-hydrogen microwave plasmas was about 1 eV; whereas, the measured neutral hydrogen temperature was 110-130 eV [14, 22]. This requires that $T_i >>> T_e$. This result can not be explained by electric field acceleration of charged species. In microwave driven plasmas, there is no high electric field in a cathode fall region ($> 1kV/cm$) to accelerate positive ions as proposed previously [18-21] to explain significant broadening in hydrogen containing plasmas driven at a high voltage electrodes. It is impossible for H or any H-containing ion which may give rise to H to have a higher temperature than the

electrons in a microwave plasma. The microwave field couples to electrons, not ions. And, the H atom temperature can not be attributed to the mechanisms proposed previously [18-21]. In fact, in the argon microwave case, the argon atoms and ions would have the highest energies since they have the largest cross section for electron collisions. No broadening of argon lines is observed. Only the hydrogen lines are broadened. The observation of excessive Balmer line broadening in a microwave driven plasma requires a source of free energy. Sources other than that provided by the electric field or known chemical reactions must be considered. We propose that the source is the energy released by the reaction which formed the rt-plasma.

We have assumed that Doppler broadening due to thermal motion was the dominant source in rt-plasmas to the extent that other sources may be neglected. To confirm this assumption, each source is now considered. In general, the experimental profile is a convolution of two Doppler profiles, an instrumental profile, the natural (lifetime) profile, Stark profiles, Van der Waals profiles, a resonance profile, and fine structure. The instrumental half-width is measured to be ±0.06 Å. The natural half-width of the Balmer α line given by Djurovic and Roberts [21] is $1.4\,X\,10^{-3}$ Å which is negligible. The fine structure splitting is also negligible.

Stark broadening of hydrogen lines in plasmas can not be measured at low electron densities using conventional emission or absorption spectroscopy because it is hidden by Doppler broadening. In the case of the Lyman α line, the Stark width exceeds the Doppler width only at $n_e > 10^{17}\,cm^{-3}$ for temperatures of about 10^4 K [23].

The relationship between the Stark broadening $\Delta\lambda_S$ of the Balmer β line in nm, the electron density n_e in m^{-3}, and the electron temperature T_e in K is

$$\log n_e = C_0 + C_1 \log(\Delta\lambda_S) + C_2[\log(\Delta\lambda_S)]^2 + C_3 \log(T_e) \qquad (3)$$

where $C_0 = 22.578$, $C_1 = 1.478$, $C_2 = -0.144$, and $C_3 = 0.1265$ [24]. From Eq. (3), to get a Stark broadening of only 1 Å with $T_e = 9000\,K$, an electron density of about $n_e \sim 3\,X\,10^{15}\,cm^{-3}$ is required compared to that of the rt-plasma of $n_e = 2\,X\,10^{9}\,cm^{-3}$ determined using a Langmuir probe as shown in Figure 8, over six orders of magnitude less. Gigosos and Cardenoso [25] give the

observed Balmer α Stark broadening for plasmas of hydrogen with helium or argon as a function of the electron temperature and density. For example, the Stark broadening of the Balmer α line recorded on a $H + He^{+}$ plasma is only 0.33 Å with $T_e = 20{,}000\,K$ and $n_e = 1.4\,X\,10^{14}\,cm^{-3}$. Thus, the Stark broadening was also insignificant.

The statistical curve fit of the $RbNO_3$ rt-plasma and hydrogen microwave plasma emission are shown in Figures 9 and 10, respectively. In each case, the data matched a Gaussian profile having the X^2 and R^2 values given in Figures 9 and 10. The absence of Stark broadening in the $RbNO_3$ rt-plasma is also evident by the good fit to a Gaussian profile rather than a Voigt profile as shown in Figure 9.

A linear Stark effect arises from an applied electric field that splits the energy level with principal quantum number n into $(2n-1)$ equidistant sublevels. The magnitude of this effect given by Videnovic et al. [18] is about $2\,X\,10^{-1}$ Å $/kV \cdot cm^{-1}$. The applied electric field was present in our study was extremely weak, 1 V/cm; thus, the linear Stark effect should be negligible.

To investigate whether the rt-plasmas of this study were optically thin or thick at a given frequency ω, the effective path length $\tau_\omega(L)$ was calculated from

$$\tau_\omega(L) = \kappa_\omega L \tag{4}$$

where L is the path length and κ_ω is the absorption coefficient given by

$$\kappa_\omega = \sigma_\omega\, X\, N_H \tag{5}$$

where σ_ω is the absorption cross section and N_H is the number density of the absorber. For optically thin plasmas $\tau_\omega(L) < 1$, and for optically thick plasmas $\tau_\omega(L) > 1$. The absorption cross section for Balmer α emission is $\sigma = 1\,X\,10^{-16}\,cm^2$ [26]. As discussed above, an estimate based on Lyman line intensity, the n=2 H atom density is $\sim 1\,X\,10^{8}\,cm^{-3}$. Since this is overwhelmingly dominated by the ground state, $N_H = 5\,X\,10^{11}\,cm^{-3}$ will be used. Thus, for a plasma length of $50\,cm$, $\tau_\omega(50\,cm)$ for Balmer α is

$$\tau_\omega(50\,cm) = \kappa_\omega L = \left(1\,X\,10^{-16}\,cm^2\right)\left(1\,X\,10^{8}\,cm^{-3}\right)(50\,cm) = 5\,X\,10^{-7} \tag{6}$$

Since $\tau_\omega(50) <<< 1$, the rt-plasmas were optically thin were optically thin; so, the self absorption of 6563 Å emission by n=2 state atomic hydrogen may be neglected as a source of the observed broadening.

Usually, the atomic hydrogen collisional cross section in plasmas is

on the order of $10^{-18}\,cm^2$ [27]. Thus, for $N_H = 5\,X\,10^{11}\,cm^{-3}$, collisional or pressure broadening is negligible.

Since the line broadening was measured with sufficient resolution (±0.06 Å) to clearly separate the RbII and KII peaks at 6555 Å and 6595 Å, respectively, from the 6563 Å Balmer α line, the possibility of a contribution of the alkali ion lines to the hydrogen line broadening was eliminated.

B. rt-plasma catalyst emission

The VUV spectrum (450 – 800 Å) of the emission of the KNO_3- H_2 gas cell is shown in Figure 11. The lines of K^+, K^{2+}, and K^{3+} corresponding to the two possible catalytic reactions were observed as reported previously [28] with the assignments confirmed by a standard potassium plasma spectrum and NIST tables [17, 29]. Line emission corresponding to K^{3+} was observed at 650 - 670 Å and 740 - 760 Å. K^{2+} was observed at 510 Å and 550 Å, and K^+ was observed at 620 Å. A large K^{3+} peak was also observed at 892 Å. K was observed at 3447 Å, 4965 Å, and 5084 Å.

The VUV spectrum (500 – 900 Å) of the emission of the $RbNO_3$- H_2 gas cell (top curve) and the standard rubidium discharge plasma (bottom curve) are shown in Figure 12. The standard rubidium discharge spectrum according to Sec. 2 is exemplary of the light source used to confirm the line assignments of each of the Group I nitrates studied. Line emission corresponding to Rb^{2+} was observed at 815.9 Å, 591 Å, 581 Å, 556 Å, and 533 Å. Rb^+ was observed at 741.5 Å, 711 Å, 697 Å, and 643.8 Å. The assignments of the Rb^{2+} and Rb^+ lines were confirmed by the NIST tables [29].

The UV spectrum (3400 – 4150 Å) of the emission of the $CsNO_3$- H_2 gas cell is shown in Figure 13. Line emission corresponding to Cs^{2+} was observed at 3477 Å, 3618 Å, and 4001 Å. Cs^+ was observed at 3680 Å, 3806 Å, and 4069 Å. Cs was observed at 3888 Å. The assignments of the Cs^{2+}, Cs^+, and Cs lines were confirmed by a standard cesium plasma spectrum and the NIST tables [29].

No plasma and no emission except blackbody radiation at long wavelengths was observed for 1.) hydrogen, argon, neon, and helium alone; 2.) sodium, magnesium, barium, and cesium metals alone, and 3.)

sodium, magnesium, and barium, with hydrogen; whereas, a bright plasma with strong VUV emission was observed in the case of cesium metal with flowing hydrogen. The VUV spectrum (400 - 800 Å) of the emission of the $CsNO_3$ - H_2 gas cell is shown in Figure 14. Line emission corresponding to the second ionization energy of cesium, $23.15745\,eV$ [12], for the decay transition Cs^{2+} to Cs^{+} was observed at 533 Å. (The 533 Å emission shown in Figure 14 is actually significantly larger than shown due to the low grating efficiency at the short wavelengths.) The only cesium lines observed for the standard cesium microwave plasma were in the visible region, and no lines were observed at wavelengths shorter than 800 Å in the case of the standard hydrogen microwave plasma.

The resonance lines of Cs II were observed with a sliding spark on the 10.7 m normal incidence vacuum spectrometer at the National Bureau of Standards (NBS) [30] as given in Table 2. The 533 Å emission of the hydrogen catalysis reaction with cesium shown in Figure 14 is dramatically different from the NBS standard cesium spectrum wherein a series of lines of Cs^{+} was observed that vanished at the limit of the ionization energy of Cs^{+} to Cs^{2+}. In fact, the ionization limit was not observed; rather, it was derived by NBS to be $23.17(4)\,eV$ [30]. Furthermore, I. S. Aleksakhin et al. recorded the emission of cesium in the 450-750 Å region during electron-atom collisions [31]. The ionization energy limit at 533 Å was not observed by I. S. Aleksakhin et al. either.

Atomic hydrogen may resonantly transfer energy to cesium to cause its double ionization to Cs^{2+}. Considering broadening by the thermal energies, the net enthalpy may be $27.2\,eV$, a match with the potential energy of atomic hydrogen; thus, it forms an rt-plasma. Cs^{2+} may then decay and emit the radiation. The vacuum reaction is

$$Cs^{2+} + e^{-} \rightarrow Cs^{+} + 23.2\,eV \tag{7}$$

Following the resonant transfer, the decay energy for the transition Cs^{2+} to Cs^{+} is predicted to give $23.2\,eV$ (533 Å) line emission corresponding to the second ionization energy of cesium, $23.15745\,eV$. This line emission was observed as shown in Figure 14 without the Rydberg series of lines of Cs^{+} as observed by NBS with a sliding spark method [30] as shown in Table 2. The observed Cs^{2+} single line emission at 533 Å supports the resonant energy transfer of $27.2\,eV$ from atomic hydrogen to atomic cesium to form an rt-plasma.

C. Hydrogen Lyman and Balmer series emission

The VUV spectra (900 – 1300 Å) of the cell emission recorded at about the point of the maximum Lyman α emission from the KNO_3, $RbNO_3$, and $CsNO_3$ gas cells are shown in Figures 15-17, respectively, with the superimposed spectrum from the hydrogen microwave plasma. Strong Lyman series VUV emission was observed only with KNO_3, $RbNO_3$, or $CsNO_3$ (or cesium metal) and hydrogen. The $CsNO_3$ emission was similar to that of the hydrogen microwave plasma; whereas, the Lyman series lines of the KNO_3 and $RbNO_3$ rt-plasmas showed population inversion with much greater intensity of atomic hydrogen versus molecular hydrogen compared to the microwave plasma emission. The population inversion was also consistent with the relative Balmer α, β, γ, and δ line intensities. Schematics of the relative intensities of the corresponding emission from the n=3, n=4, n=5, and n=6 state to the n=2 state recorded on a hydrogen microwave plasma, a KNO_3 rt-plasma, and a $RbNO_3$ rt-plasma are shown in Figure 18, 19, and 20, respectively.

The Lyman population density of the excited hydrogen atoms N_α, N_β, and N_γ with principal quantum numbers $n = 2,3,\text{and } 4$, respectively, were obtained from their intensity integrated over the spectral peaks corrected by their Einstein coefficients. The population ratios, $\frac{N_\beta}{N_\alpha}$ and $\frac{N_\gamma}{N_\alpha}$, for pure H_2 and H_2 with KNO_3 or $RbNO_3$ are given in Table 3.

The important parameter for a lasing medium is the reduced population density $\frac{N}{g}$ given by the population density N divided by the statistical weight g as discussed by Akatsuka et al. [6]. The ratio of $\frac{N}{g}$ for L_β to L_α and L_γ to L_α given in Table 4 demonstrate that with appropriate cavity length and mirror reflection coefficient cw laser oscillations may be obtained between $n = 3$ and $n = 2$ since the corresponding $\frac{N_\beta}{N_\alpha}\frac{g_\alpha}{g_\beta} > 1$ [6]. Lasing further requires an overpopulation which may be determined from the absolute intensity of the Balmer α line.

From the population ratios, $\frac{N_\beta}{N_\alpha}$ ($\frac{N_3}{N_2}$) and $\frac{N_\gamma}{N_\alpha}$ ($\frac{N_4}{N_2}$), shown in Table 3, the corresponding $\frac{N_4}{N_3}$ was determined to be 0.78, 0.74, and 0.29 for the hydrogen microwave plasma, KNO_3 rt-plasma, and $RbNO_3$ rt-plasma, respectively. Whereas, from the Balmer line intensities, $\frac{N_4}{N_3}$ was determined to be 0.78, 0.76, and 0.29 for the hydrogen microwave plasma, KNO_3 rt-plasma, and $RbNO_3$ rt-plasma, respectively. Since $\frac{N_4}{N_3}$ determined from the Lyman series and the Balmer series were the same and the Balmer α line was absolutely measured, the absolute reduced number densities for n=2 to n=6 was determined from the absolute Balmer α line intensity (absolute $\frac{N_3}{g_3}$ where the experimental $N_3 \sim 1.25 X 10^8\ cm^{-3}$) and the relative ratio of the Lyman and Balmer series lines. A plot of the absolute reduced population density $\frac{N_n}{g_n}$ versus quantum number n recorded on a hydrogen microwave plasma, a KNO_3 rt-plasma, and a $RbNO_3$ rt-plasma is shown in Figure 21. An inverted population was only observed for n=3 in the case of KNO_3 and $RbNO_3$ rt-plasmas.

For the plasma conditions of this experiment ($T_e = 0.7 - 0.8\ eV$, $n_e \approx 10^9\ cm^{-3}$), a threshold reduced overpopulation of $4.4 X 10^6\ cm^{-3}$ is required for lasing assuming a cavity length of 100 cm and a mirror reflection coefficient of 0.99. Modeling results based on the collisional-radiative model [6] given in Sec. 3D show that the threshold condition is achievable for these plasmas. Due to the short lifetime of the Balmer α line, an exceptionally monochromatic laser with the possibility of fast switching is anticipated.

Other explanations of the over population were ruled out. The spectrometer response was determined to be approximately flat in the 1000-1300 Å region. To investigate whether the rt-plasmas of this study were optically thin or thick at 1216 Å, the effective path length $\tau_\omega(50\ cm)$ was calculated from Eq. (6) using the absorption cross section for Lyman α emission, $\sigma = 4 X 10^{-16}\ cm^2$ [26], and $N_H = 5 X 10^{11}\ cm^{-3}$.

$$\tau_\omega(50\ cm) = \kappa_\omega L = \left(4 X 10^{-16}\ cm^2\right)\left(5 X 10^{11}\ cm^{-3}\right)(50\ cm) = 1 X 10^{-2} \qquad (8)$$

Since $\tau_\omega(50) <<< 1$, the rt-plasmas were optically thin; so, the self absorption of 1216 Å emission by n=1 state atomic hydrogen may be neglected as the cause of the inverted ratio. Furthermore, the L_α / L_β intensity ratios of the control hydrogen plasmas closely matched the NIST intensity ratio using the NIST Einstein A coefficients [17]. Since the hydrogen pressure was the same in the rt-plasmas and the control hydrogen plasma, the same Einstein A coefficients were used to calculate the number density ratio in both cases.

In a non-recombining plasma [6], thermal electron collisional mechanisms can not produce the conditions necessary for population inversion. The highly ionized alkali ions observed in the plasma may ionize atomic hydrogen which may recombine in an excited state; yet, no such reaction has ever been observed which gives rise to an inverted Lyman population. Neither electrical ionization nor chemical ionization is known to form an inverted Lyman population. All known sources of excitation were exhausted [32]. The observation, then, of population inversion indicates the presence of free energy in the system. This is further evidence that a new chemical source of energy, greater than 12 eV/atom was present as is the observation of ions such as K^{3+} which requires an energy source of at least $81.7766\,eV$. The only possibility known to the authors is the proposed rt-plasma reaction [7].

T_e was determined to be $0.84\,eV$ and $0.76\,eV$ for the K^+ and Rb^+ rt-plasma respectively. Similarly, $k_B T_e = (0.30 - 0.43)\,eV$ was determined for a K^+ rt-plasma as reported by Conrads et al. [32] with the assumption of a Maxwell Boltzmann distribution of the level population, and a slightly higher temperature of $k_B T_e = (0.32 - 0.48)\,eV$ was found when a corona model was applied. The data indicated that the electron temperature was not higher than $k_B T_e = 0.5\,eV$. On this basis, it was astonishing that a strong Lyman beta transition appeared in the spectra since an excitation energy of $12.1\,eV$ is required. This energy is a factor of about 25 above the measured thermal energy. The amount of electrons in the Maxwell tail that had enough energy to enhance the Lyman transition was 11 orders of magnitude lower than the total number of electrons. Longer range fields (of the order of mm) were only about a 1 V/cm. In addition to electron collisional excitation, known chemical reactions, resonant photon transfer, and multiphoton absorption, and the lowering of the ionization

and excitation energies by the state of "non ideality" in dense plasmas were also rejected as the source of ionization or excitation to form the hydrogen plasma.

A source of energy other than that provided by the electric field or known chemical reactions must be considered. We propose that the plasma formed chemically rather than electrically and that the product of the energetic chemical reaction of atomic hydrogen with potassium or rubidium ions which serve as catalysts as well as reactants are compounds having novel hydride ions reported previously [33]. Prior related studies that support the possibility of a novel reaction of atomic hydrogen which produces a chemically generated or assisted plasma (rt-plasma) and produces novel hydride compounds include VUV spectroscopy [7-8, 13-14, 28, 32-41], characteristic emission from catalysts and the hydride ion products [28, 32, 37-38], lower-energy hydrogen emission [13, 36-38], chemically formed plasmas [7-8, 28, 32-33, 37-40], Balmer α line broadening [8, 14, 32-35, 41], elevated electron temperature [14, 34-35], anomalous plasma afterglow duration [40], power generation [34-35, 39, 41-42], and analysis of novel chemical compounds [43-44].

The predicted catalyst ion emission was observed from rt-plasmas as presented in Sec. 3B. For example, characteristic emission was observed from K^{2+} as well as K^{3+} which confirmed the resonant energy transfer of $27.2\,eV$ and $3 \cdot 27.2\,eV$, respectively, from atomic hydrogen to the catalyst K^+ / K^+ and K, respectively. With a highly conductive plasma, the voltage of the cell was about 20 V, and the field strength was about 1-2 V/cm which was too low to ionize potassium to K^{3+} which requires at least $81.7766\,eV$. Similarly, the ionization of K^+ to K^{2+} requires $31.63\,eV$ which could not have been due to the weak electric field. Known chemical reactions are also of too low an energy by at least an order of magnitude to form K^{2+} and K^{3+}. The K^{3+} lines generated in the incandescently heated cell and due to the catalyst reaction of atomic hydrogen were confirmed by a high voltage discharge and NIST tables [17, 29].

Then the inverted population is explained by a further resonance energy transfer from the short-lived highly energetic intermediates formed by the rt-plasma reactions to yield $H(n>2)$ atoms directly by

multipole coupling [34] and fast $H(n=1)$ atoms. The emission of $H(n=3)$ from fast $H(n=1)$ atoms excited by collisions with the background H_2 has been discussed by Radovanov et al. [45]. Formation of H^+ is also predicted which is far from thermal equilibrium in terms of the hydrogen atom temperature as discussed in Sec. 3C and modeled in Sec. 3D. Akatsuka et al. [6] show that it is characteristic of cold recombining plasmas to have the high lying levels in local thermodynamic equilibrium (LTE); whereas, for the low lying levels, population inversion is obtained when T_e becomes low with an appropriate electron density as shown by the Saha-Boltzmann equation.

D. Level Population Model and Lasing Ability

In order to estimate hydrogen excited state level populations and assess lasing ability, the collisional radiative model [6, 46] is applied to the plasma conditions obtained herein ($T_e \sim 0.8\,eV$, $n_e \sim 10^9\,cm^{-3}$). The collisional radiative model explicitly includes all level population and de-population mechanisms for each excited level from every other excited level in the hydrogen atom. Excited level n is, then, populated by collisional excitation from all lower excited states, and collisional and radiative de-excitation from all higher excited states. De-population explicitly includes collisional and radiative de-excitation to all lower states, and collisional excitation to all higher levels. Independent ionization loss, radiative recombination, and dielectronic recombination are included for all levels as well. A separate balance equation is prescribed for each individual level and is coupled to all other level equations through the population and de-population terms described above.

In order to close the set of equations, truncation was chosen at n=5. This is justified by both the experimental observation of very low measurable emission from higher lying states and *a posteriori* via the model results indicating a progression of negligibly smaller level densities beyond n=3. The ground state (n=1) level population cannot be determined by this method since the important affects of dissociation, molecular recombination, and transport are not included. As discussed earlier (Sec. 3A), however, an estimate based on emission line profiles

places the total H atom density $\sim 5 X 10^{11} cm^{-3}$. Since this is overwhelmingly dominated by the ground state, the assignment $N_1 = 5 X 10^{11} cm^{-3}$ will be made throughout.

Solution to the n=2 – 5 level equations under these conditions shows no inversion in any of the level populations. This is an expected result for a steady, thermal plasma. Also, as expected, the dominant mechanisms are found to be population by collisional excitation and de-population by radiative decay.

The results of this calculation ($N_{2-5} < 10^4 cm^{-3}$) are inconsistent with the spectroscopic observations. Absolutely calibrating the monochromator near H_α however yields, $N_3 \sim 1.25 X 10^8 cm^{-3}$. There is, then, a heretofore undetermined mechanism providing direct excited state population, *i.e.* pumping. To help quantify the affects of this mechanism, the level equations are once again evaluated with N_3 fixed to $1.25 X 10^8 cm^{-3}$ and the inclusion of an independent pumping rate. Since spectroscopic results indicate n=3 – 2 inversion, pumping is prescribed to the n=3 state from the ground state, n=1. The results from this calculation for n=1 – 5 are summarized in Table 5.

Now collisional mechanisms from the n=3 state as well as ground state collisional excitation and radiative decay significantly contribute to population and de-population rates. In addition, a demonstrated inversion in the population between the n=3 and 2 states is predicted. The reduced overpopulation density for this case is $D(N/g) \sim 4.7 X 10^6 cm^{-3}$, slightly above the threshold of $4.4 X 10^6 cm^{-3}$. The pumping rate is also determined in this analysis yielding a rate of $\sim 6.44 X 10^{16} cm^{-3} s^{-1}$. Since the n=3 state has a excitation energy of $12.08 eV$, the pumping mechanism consumes energy at a rate of $\sim 0.124 W \cdot cm^{-3}$, which is returned as H_α and H_β radiation.

4. Conclusion

$2K^+$ to $K + K^{2+}$, Rb^+ to Rb^{2+}, and Cs to Cs^{2+} each provide a reaction with a net enthalpy equal to the potential energy of atomic hydrogen, $27.2 eV$, and K to K^{3+} provides a reaction with a net enthalpy equal to $3 \cdot 27.2 eV$. The presence of these gaseous atoms and ions with thermally dissociated hydrogen formed a plasma having strong VUV emission.

Emission was observed from Rb^{+}, Rb^{2+}, K, K^{+}, K^{2+}, K^{3+}, Cs, Cs^{+}, and Cs^{2+} that confirmed the resonant energy transfer with the formation of the corresponding rt-plasma. Emission was also observed from a continuum state of Cs^{2+} at 533 Å. The single emission feature with the absence of the other corresponding Rydberg series of lines from species confirmed the resonant energy transfer of $27.2\,eV$ from atomic hydrogen to atomic cesium.

A stationary inverted Lyman population was observed with potassium and rubidium catalysts. The ionization and population of excited atomic hydrogen levels was attributed to energy provided by the rt-plasma reactions. The high hydrogen atom temperature with a relatively low electron temperature, $T_e < 1\,eV$, were characteristic of cold recombining plasmas [6]. These conditions of the rt-plasmas favored an inverted population in the lower levels. Thus, the catalysis of atomic hydrogen may pump a cw HI laser. From our results, laser oscillations are expected between $n = 3$ and $n = 2$.

References

1. C. Zimmermann, R. Kallenbach, T. W. Hansch, Phys. Rev. Lett., Vol. 65, (1990), p. 571.
2. T. Ibuki, Chem. Phys. Lett., Vol. 94, (1990), p. 169.
3. L. I. Gudzenko, L. A. Shelepin, Sov. Phys. JEPT, Vol. 18, (1963), p. 998.
4. S. Suckewer, H. Fishman, J. Appl. Phys., Vol. 51, (1980), p. 1922.
5. W. T. Silfvast, O. R. Wood, J. Opt. Soc. Am. B, Vol. 4, (1987), p. 609.
6. H. Akatsuka, M. Suzuki, "Stationary population inversion of hydrogen in arc-heated magnetically trapped expanding hydrogen-helium plasma jet", Phys. Rev. E, Vol. 49, (1994), pp. 1534-1544.
7. R. Mills, J. Dong, Y. Lu, "Observation of Extreme Ultraviolet Hydrogen Emission from Incandescently Heated Hydrogen Gas with Certain Catalysts", Int. J. Hydrogen Energy, Vol. 25, (2000), pp. 919-943.
8. R. Mills and M. Nansteel, P. Ray, "Argon-Hydrogen-Strontium Discharge Light Source", IEEE Transactions on Plasma Science, in press.
9. R. Mills, *The Grand Unified Theory of Classical Quantum Mechanics*, September 2001 Edition, BlackLight Power, Inc., Cranbury, New Jersey, Distributed by Amazon.com; posted at www.blacklightpower.com.
10. R. Mills, "The Grand Unified Theory of Classical Quantum Mechanics",

Int. J. Hydrogen Energy, Vol. 27, No. 5, (2002), pp. 565-590.
11. R. Mills, "The Nature of Free Electrons in Superfluid Helium--a Test of Quantum Mechanics and a Basis to Review its Foundations and Make a Comparison to Classical Theory", Int. J. Hydrogen Energy, Vol. 26, No. 10, (2001), pp. 1059-1096.
12. David R. Linde, *CRC Handbook of Chemistry and Physics*, 79 th Edition, CRC Press, Boca Raton, Florida, (1998-9), p. 10-175 to p. 10-177.
13. R. Mills, P. Ray, "Spectral Emission of Fractional Quantum Energy Levels of Atomic Hydrogen from a Helium-Hydrogen Plasma and the Implications for Dark Matter", Int. J. Hydrogen Energy, Vol. 27, No. 3, pp. 301-322.
14. R. L. Mills, P. Ray, B. Dhandapani, J. He, "Comparison of Excessive Balmer α Line Broadening of Glow Discharge and Microwave Hydrogen Plasmas with Certain Catalysts", Chem. Phys., submitted.
15. H. R. Griem, *Principle of Plasma Spectroscopy*, Cambridge University Press, (1987).
16. J. Tadic, I. Juranic, G. K. Moortgat, "Pressure dependence of the photooxidation of selected carbonyl compounds in air: n-butanal and n-pentanal", J. Photochemistry and Photobiology A: Chemistry, Vol. 143, (2000), 169-179.
17. NIST Atomic Spectra Database, www.physics.nist.gov/cgi-bin/AtData/display.ksh.
18. I. R. Videnovic, N. Konjevic, M. M. Kuraica, "Spectroscopic investigations of a cathode fall region of the Grimm-type glow discharge", Spectrochimica Acta, Part B, Vol. 51, (1996), pp. 1707-1731.
19. M. Kuraica, N. Konjevic, "Line shapes of atomic hydrogen in a plane-cathode abnormal glow discharge", Physical Review A, Volume 46, No. 7, October (1992), pp. 4429-4432.
20. S. B. Radovanov, K. Dzierzega, J. R. Roberts, J. K. Olthoff, "Time-resolved Balmer-alpha emission from fast hydrogen atoms in low pressure, radio-frequency discharges in hydrogen", Appl. Phys. Letts., Vol. 66, No. 20, (1995), pp. 2637-2639.
21. S. Djurovic, J. R. Roberts, "Hydrogen Balmer alpha line shapes for hydrogen-argon mixtures in a low-pressure rf discharge", J. Appl. Phys., Vol. 74, No. 11, (1993), pp. 6558-6565.

22. R. L. Mills, P. Ray, "Substantial Changes in the Characteristics of a Microwave Plasma Due to Combining Argon and Hydrogen", New Journal of Physics, in press.
23. J. Seidel, "Theory of two-photon polarization spectroscopy of plasma-broadened hydrogen L_α line", Phys. Rev. Letts., Vol. 57, No. 17, (1986), p. 2154.
24. A. Czernikpwski, J. Chapelle, Acta Phys. Pol. A., Vol. 63, (1983), p. 67.
25. M. A. Gigosos, V. Cardenoso, "New plasma diagnosis tables of hydrogen Stark broadening including ion dynamics", J. Phys. B: At. Mol. Opt. Phys., Vol. 29, (1996), pp. 4795-4838.
26. H. Okabe, *Photochemistry of Small Molecules*, John Wiley & Sons, New York, (1978).
27. A. Corney, Atomic and Laser Spectroscopy, Clarendon Press, Oxford, (1977).
28. R. Mills, P. Ray, "Spectroscopic Identification of a Novel Catalytic Reaction of Potassium and Atomic Hydrogen and the Hydride Ion Product", Int. J. Hydrogen Energy, Vol. 27, No. 2, (2002), pp. 183-192.
29. R. Kelly, Journal of Physical and Chemical Reference Data. "Atomic and Ionic Spectrum Lines below 2000 Angstroms: Hydrogen through Krypton", Part I (H-Cr), Volume 16, (1987), Supplement No. 1, Published by the American Chemical Society and the American Institute of Physics for the National Bureau of Standards, pp. 418-422.
30. J. Reader, G. L. Epstein, "Resonance lines of Cs II, Ba III, and La IV", Journal of the Optical Society of America, Vol. 65, No. 6, June, (1975), pp. 638-641.
31. I. S. Aleksakhin, G. G. Bogachev, A. I. Zapesochnyi, "Study of the emission of potassium, rubidium, and cesium in the 45-75 nm region during electron-atom collisions", J. Applied Spectroscopy, Vol. 23, No. 6, December, (1975), pp. 1666-1668. Translated from Zh. Prikl. Spektrosk. (USSR), Vol. 23, No. 6, December (1975), pp. 1103-1105.
32. H. Conrads, R. Mills, Th. Wrubel, "Emission in the Deep Vacuum Ultraviolet from an Incandescently Driven Plasma in a Potassium Carbonate Cell", Plasma Sources Science and Technology, submitted.
33. R. L. Mills, P. Ray, "A Comprehensive Study of Spectra of the Bound-Free Hyperfine Levels of Novel Hydride Ion $H^-(1/2)$, Hydrogen, Nitrogen, and Air", Int. J. Hydrogen Energy, in press.

34. R. L. Mills, P. Ray, B. Dhandapani, J. He, "Spectroscopic Identification of Fractional Rydberg States of Atomic Hydrogen", J. of Phys. Chem., submitted.
35. R. L. Mills, P. Ray, B. Dhandapani, M. Nansteel, X. Chen, J. He, "New Power Source from Fractional Rydberg States of Atomic Hydrogen", Chem. Phys. Letts., in press.
36. R. Mills, P. Ray, "Vibrational Spectral Emission of Fractional-Principal-Quantum-Energy-Level Hydrogen Molecular Ion", Int. J. Hydrogen Energy, Vol. 27, No. 5, (2002), pp. 533-564.
37. R. Mills, "Spectroscopic Identification of a Novel Catalytic Reaction of Atomic Hydrogen and the Hydride Ion Product", Int. J. Hydrogen Energy, Vol. 26, No. 10, (2001), pp. 1041-1058.
38. R. L. Mills, P. Ray, "Spectroscopic Identification of a Novel Catalytic Reaction of Rubidium Ion with Atomic Hydrogen and the Hydride Ion Product", Int. J. Hydrogen Energy, in press.
39. R. Mills and M. Nansteel, P. Ray, "Argon-Hydrogen-Strontium Discharge Light Source", IEEE Transactions on Plasma Science, April, (20002) issue.
40. R. Mills, T. Onuma, and Y. Lu, "Formation of a Hydrogen Plasma from an Incandescently Heated Hydrogen-Catalyst Gas Mixture with an Anomalous Afterglow Duration", Int. J. Hydrogen Energy, Vol. 26, No. 7, July, (2001), pp. 749-762.
41. R. L. Mills, P. Ray, "Substantial Changes in the Characteristics of a Microwave Plasma Due to Combining Argon and Hydrogen", New Journal of Physics, www.njp.org, Vol. 4, (2002), pp. 22.1-22.17.
42. R. Mills, N. Greenig, S. Hicks, "Optically Measured Power Balances of Anomalous Discharges of Mixtures of Argon, Hydrogen, and Potassium, Rubidium, Cesium, or Strontium Vapor", Int. J. Hydrogen Energy, Vol. 27, No. 6, (2002), pp. 651-670.
43. R. Mills, B. Dhandapani, M. Nansteel, J. He, T. Shannon, A. Echezuria, "Synthesis and Characterization of Novel Hydride Compounds", Int. J. of Hydrogen Energy, Vol. 26, No. 4, (2001), pp. 339-367.
44. R. Mills, B. Dhandapani, N. Greenig, J. He, "Synthesis and Characterization of Potassium Iodo Hydride", Int. J. of Hydrogen Energy, Vol. 25, Issue 12, December, (2000), pp. 1185-1203.
45. S. B. Radovanov, K. Dzierzega, J. R. Roberts, J. K. Olthoff, "Time-resolved

Balmer-alpha emission from fast hydrogen atoms in low pressure, radio-frequency discharges in hydrogen", Appl. Phys. Lett., Vol. 66, No. 20, (1995), pp. 2637-2639.

46. T. Fujimoto, J. Phys. Soc. Jpn., Vol. 47, (1979). p. 265.

Figure Captions

Figure 1. The experimental set up comprising a filament gas cell to form an rt-plasma light source and an VUV spectrometer which was differentially pumped.

Figure 2. The 6563 Å Balmer α line width recorded with a high resolution (±0.06 Å) visible spectrometer on an rt-plasma formed with K and K^+/K^+ catalysts. Significant broadening was observed corresponding to an average hydrogen atom temperature of $18\,eV$.

Figure 3. The 6563 Å Balmer α line width recorded with a high resolution (±0.06 Å) visible spectrometer on an rt-plasma formed with Rb^+ catalyst. Significant broadening was observed corresponding to an average hydrogen atom temperature of $12\,eV$.

Figure 4. The 6563 Å Balmer α line width recorded with a high resolution (±0.06 Å) visible spectrometer on an rt-plasma formed with Cs catalyst. Significant broadening was observed corresponding to an average hydrogen atom temperature of $12\,eV$.

Figure 5. The 4861 Å Balmer β line width recorded with a high resolution (±0.06 Å) visible spectrometer on an rt-plasma formed with Rb^+ catalyst. Significant broadening was observed corresponding to an average hydrogen atom temperature of $12\,eV$.

Figure 6. The 4340 Å Balmer γ line width recorded with a high resolution (±0.06 Å) visible spectrometer on an rt-plasma formed with Rb^+ catalyst. Significant broadening was observed corresponding to an average hydrogen atom temperature of $14\,eV$.

Figure 7. The 4102 Å Balmer δ line width recorded with a high resolution (±0.06 Å) visible spectrometer on an rt-plasma formed with Rb^+ catalyst. Significant broadening was observed corresponding to an average hydrogen atom temperature of $11\,eV$.

Figure 8. The probe current versus voltage trace of the Langmuir probe of the $RbNO_3$ rt-plasma. The electron density and temperature were measured to be $n_e = 2X10^9\,cm^{-3}$ and $T_e = 1-2\,eV$. The electron density was over six orders of magnitude less than that required to achieve 1 Å electron Stark broadening.

Figure 9. The statistical curve fit of an $RbNO_3$ rt-plasma. The data

matched a Gaussian profile having the $X^2 = \sum \frac{(\text{Calculated} - \text{Measured})^2}{\text{Calculated}}$ and R^2 (correlation coefficient squared) values of 0.00023 and 0.99908, respectively. Significant broadening was observed corresponding to an average hydrogen atom temperature of $12\,eV$.

Figure 10. The statistical curve fit of the hydrogen microwave plasma. The data matched a Gaussian profile having the X^2 and R^2 values of 0.00092 and 0.98937, respectively.

Figure 11. The VUV spectrum (450 – 800 Å) of the cell emission recorded at about the point of the maximum Lyman α emission from a gas cell at a cell temperature of 700 °C comprising a tungsten filament, a titanium dissociator, 300 mtorr hydrogen, and vaporized K and K^+ from KNO_3 that was recorded with a CEM. Line emission corresponding to K^{3+} was observed at 650 - 670 Å and 740 - 760 Å. K^{2+} was observed at 510 Å and 550 Å, and K^+ was observed at 620 Å.

Figure 12. The VUV spectrum (500 – 900 Å) of the emission of the $RbNO_3$ - H_2 gas cell (top curve) and the standard rubidium plasma (bottom curve). The $RbNO_3$ - H_2 gas cell comprised a tungsten filament, a titanium dissociator, 300 mTorr hydrogen, and vaporized Rb^+ from $RbNO_3$. The emission was recorded with a CEM at about the point of the maximum Lyman α at a cell temperature of 700 °C. Line emission corresponding to Rb^{2+} was observed at 815.9 Å, 591 Å, 581 Å, 556 Å, and 533 Å. Rb^+ was observed at 741.5 Å, 711 Å, 697 Å, and 643.8 Å.

Figure 13. The UV spectrum (3400 – 4150 Å) the cell emission recorded at about the point of the maximum Lyman α emission from a gas cell at a cell temperature of 700 °C comprising a tungsten filament, a titanium dissociator, 300 mtorr hydrogen, and vaporized Cs from $CsNO_3$ that was recorded with a photomultiplier tube (PMT) and a sodium salicylate scintillator. Line emission corresponding to Cs^{2+} was observed at 3477 Å, 3618 Å, and 4001 Å. Cs^+ was observed at 3680 Å, 3806 Å, and 4069 Å. Cs was observed at 3888 Å.

Figure 14. The VUV spectrum (400 – 800 Å) of the cell emission from the gas cell at a cell temperature of 700 °C comprising a tungsten filament, vaporized cesium metal, and 300 mtorr hydrogen that was recorded with a PMT and a sodium salicylate scintillator. Emission was observed from a continuum state of Cs^{2+} at 533 Å. The single emission

feature with the absence of the other corresponding Rydberg series of lines from Cs^+ confirmed the resonant energy transfer of $27.2\,eV$ from atomic hydrogen to atomic cesium.

Figure 15. The VUV spectra (900 - 1300 Å) of the cell emission from hydrogen microwave plasma (dotted line) and the KNO_3-H_2 rt-plasma (solid line) with an inverted Lyman population.

Figure 16. The VUV spectra (900 - 1300 Å) of the cell emission from hydrogen microwave plasma (dotted line) and the $RbNO_3$-H_2 rt-plasma (solid line) with an inverted Lyman population.

Figure 17. The VUV spectra (900 - 1300 Å) of the cell emission from hydrogen microwave plasma (dotted line) and the $CsNO_3$-H_2 rt-plasma (solid line) with no inverted Lyman population.

Figure 18. A schematic of the relative Balmer α, β, γ, and δ line intensities corresponding to n=3, n=4, n=5, and n=6 recorded on a hydrogen microwave plasma.

Figure 19. A schematic of the relative Balmer α, β, γ, and δ line intensities corresponding to n=3, n=4, n=5, and n=6 recorded on a KNO_3 rt-plasma.

Figure 20. A schematic of the relative Balmer α, β, γ, and δ line intensities corresponding to n=3, n=4, n=5, and n=6 recorded on a $RbNO_3$ rt-plasma.

Figure 21. A plot of the absolute reduced population density $\frac{N_n}{g_n}$ versus quantum number n recorded on a hydrogen microwave plasma, a $RbNO_3$ rt-plasma, and a KNO_3 rt-plasma. In the case of KNO_3 and $RbNO_3$ rt-plasmas, population inversion was observed for n=3. From a collisional-radiative model, an overpopulation was achieved for n=3 .

Table 1. Energetic hydrogen atom densities and energies for rt-plasmas determined from the 6563 Å Balmer α line width.

Plasma Gas	Hydrogen Atom Density[a] (10^{11} $atoms/cm^3$)	Hydrogen Atom Energy[b] (eV)
H_2	2	2-3[c]
$K;K^+/K^+/H_2$	4	15-18
Rb^+/H_2	6	9-12
Cs/H_2	4	10-12

[a] Approximate Calculated after [18].

[b] Calculated after [18].

[c] Measured on a microwave discharge after [14].

Table 2. Resonance lines of Cs II observed with a sliding spark on the 10.7 m normal incidence vacuum spectrometer at NBS [30]. The uncertainty of the wavelengths is ±0.005 Å.

λ (Å)	Intensity	σ (cm^{-1})	Upper Level
926.657	40000	107914.8	$6p^6 5d\ ^3P_1$
901.270	35000	110954.5	$6s3/2[3/2]_1$
813.837	15000	122874.7	$6s1/2[1/2]_1$
808.761	15000	123645.9	$5d\ ^3D_1$
718.138	15000	139249.0	$5d\ ^1P_1$
668.386	500	149614	$7s3/2[3/2]_1$
657.112	100	152181	$6d\ ^3P_1$
639.356	2000	156407	$6d\ ^3D_1$
612.756	35	163189	$7s1/2[1/2]_1$
591.044	250	169192	$6d\ ^1P_1$
607.291	50	164666	$8s3/2[3/2]_1$
575.320	10	173816	$6d\ ^3D_1$
564.158	1	177256	$7d\ ^1P_1$

Table 3. The population density ratios $\frac{N_\beta}{N_\alpha}$ and $\frac{N_\gamma}{N_\alpha}$ for pure H_2, KNO_3, and $RbNO_3$.

Plasma Gas	$\frac{N_\beta}{N_\alpha}$	$\frac{N_\gamma}{N_\alpha}$
Pure H_2 [a]	0.664	0.521
KNO_3	4.72	3.48
$RbNO_3$	4.30	1.26

[a] Measured on microwave discharge maintained after [13-14].

Table 4. The reduced population density ratios $\frac{N}{g}$ for pure H_2, KNO_3, and $RbNO_3$.

Plasma Gas	$\frac{N_\beta}{N_\alpha}\frac{g_\alpha}{g_\beta}$ a	$\frac{N_\gamma}{N_\alpha}\frac{g_\alpha}{g_\gamma}$ b
Pure H_2 [c]	0.292	0.130[c]
KNO_3	2.07	0.870
$RbNO_3$	1.89	0.314

a $\frac{g_\alpha}{g_\beta} = 0.444$ where $g = 2n^2$ and n is the principal quantum number

b $\frac{g_\alpha}{g_\gamma} = 0.250$

[c] Measured on microwave discharge after [14].

Table 5. Level densities N_n for excited states n=1 – 5 with an n=3 pumping mechanism.

n	$N_n(10^8\ cm^{-3})$
1	5000
2	0.18
3	1.25
4	0.000229
5	0.000138

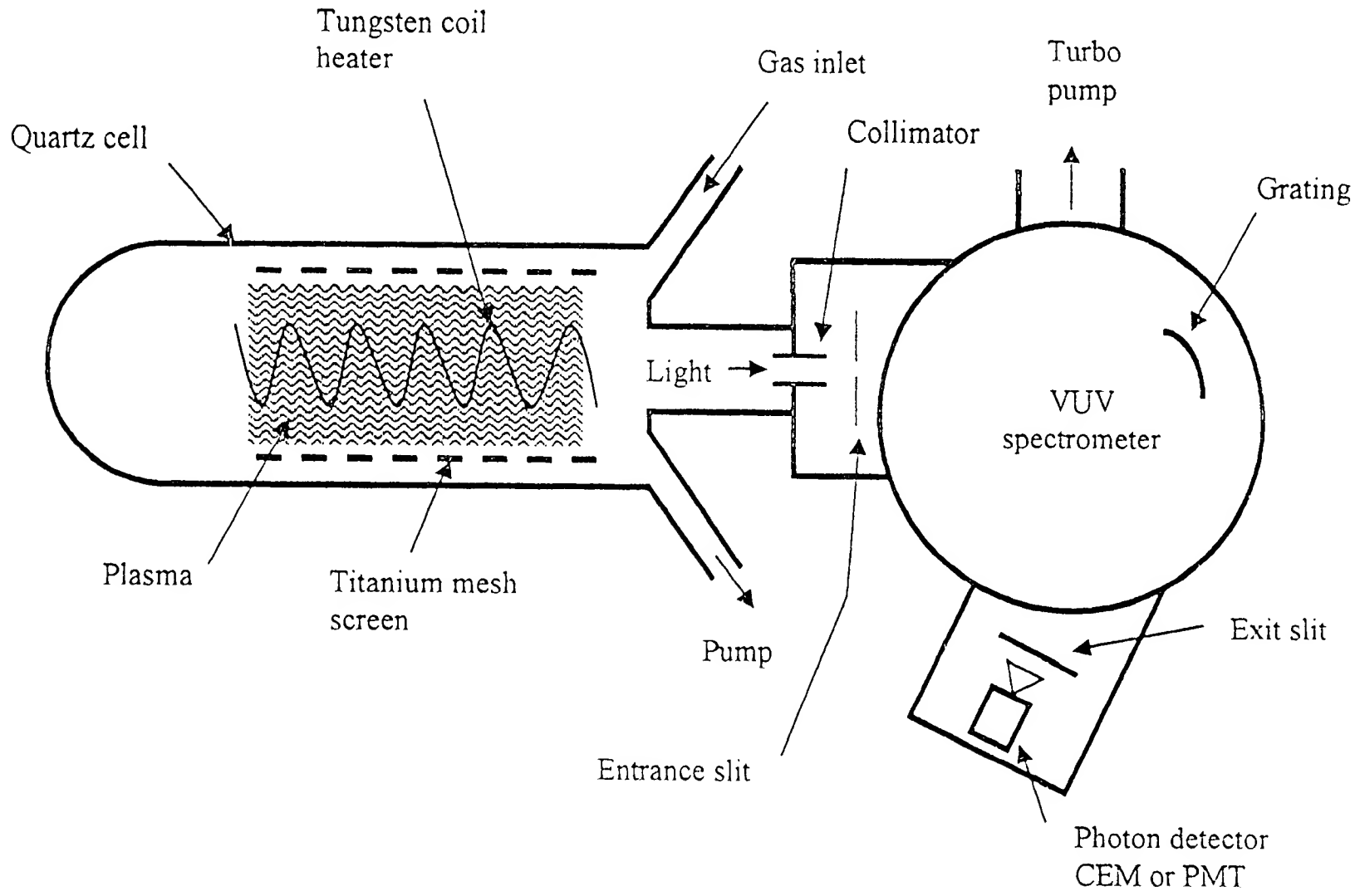
Tungsten coil heater
Gas inlet
Turbo pump
Quartz cell
Collimator
Grating
Light
VUV spectrometer
Plasma
Titanium mesh screen
Pump
Exit slit
Entrance slit
Photon detector CEM or PMT

Fig. 1

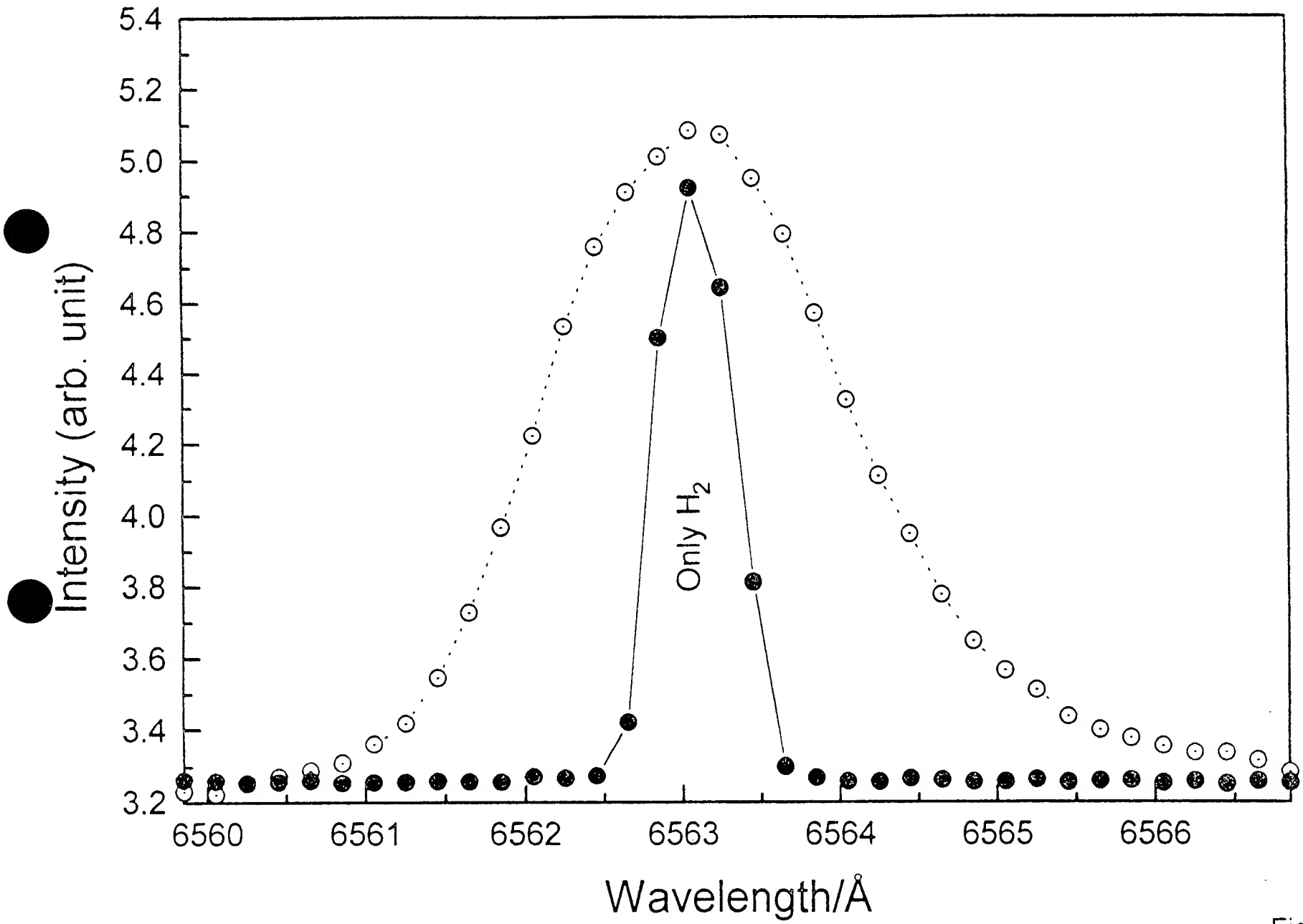
5.4
5.2
5.0
4.8
4.6
4.4
4.2
4.0
3.8
3.6
3.4
3.2
Intensity (arb. unit)
Only H_2
6560
6561
6562
6563
6564
6565
6566
Wavelength/Å

Fig. 2

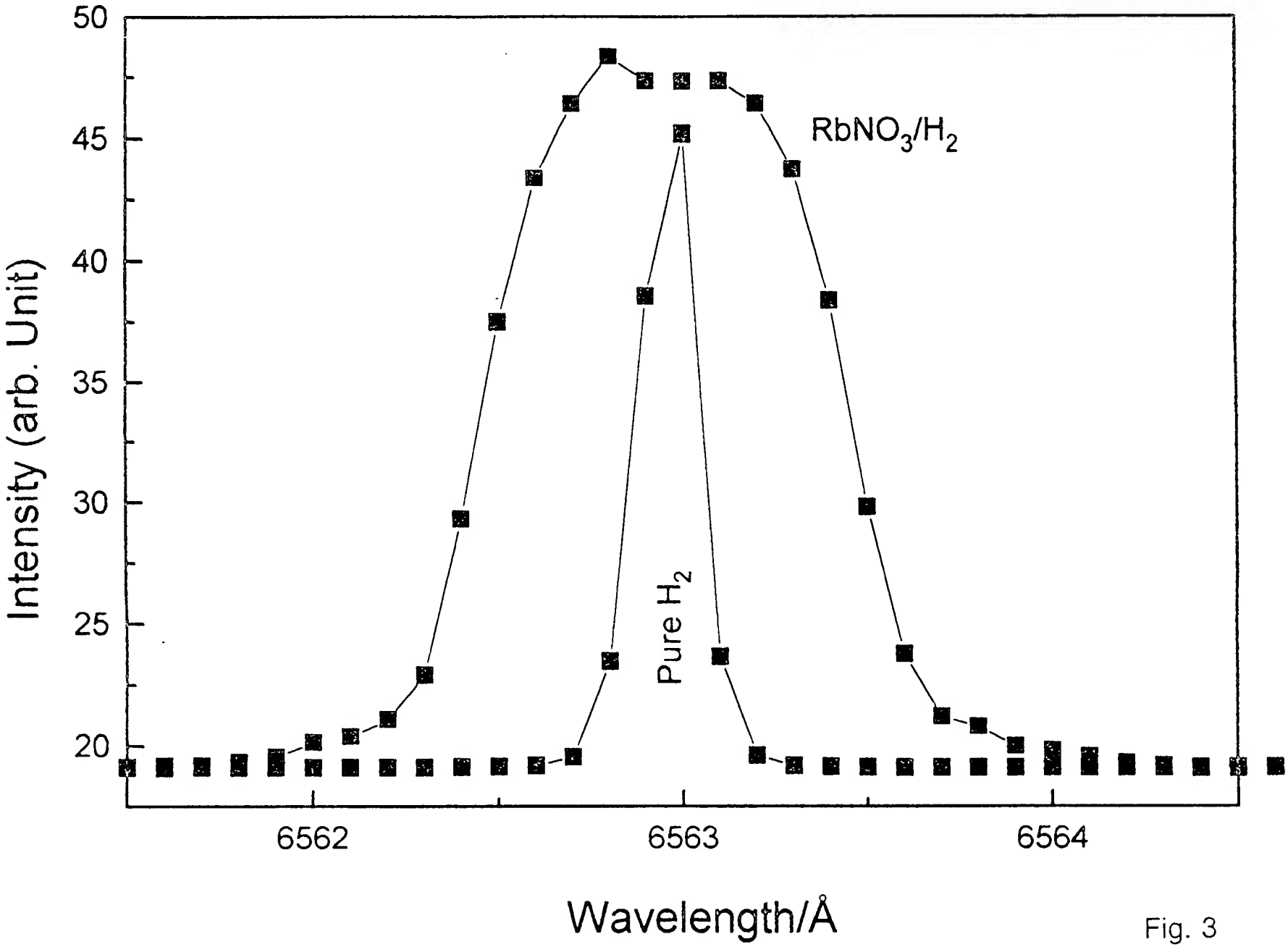
50
45
40
35
30
25
20
Intensity (arb. Unit)
RbNO3/H2
Pure H2
6562
6563
6564
Wavelength/Å

Fig. 3

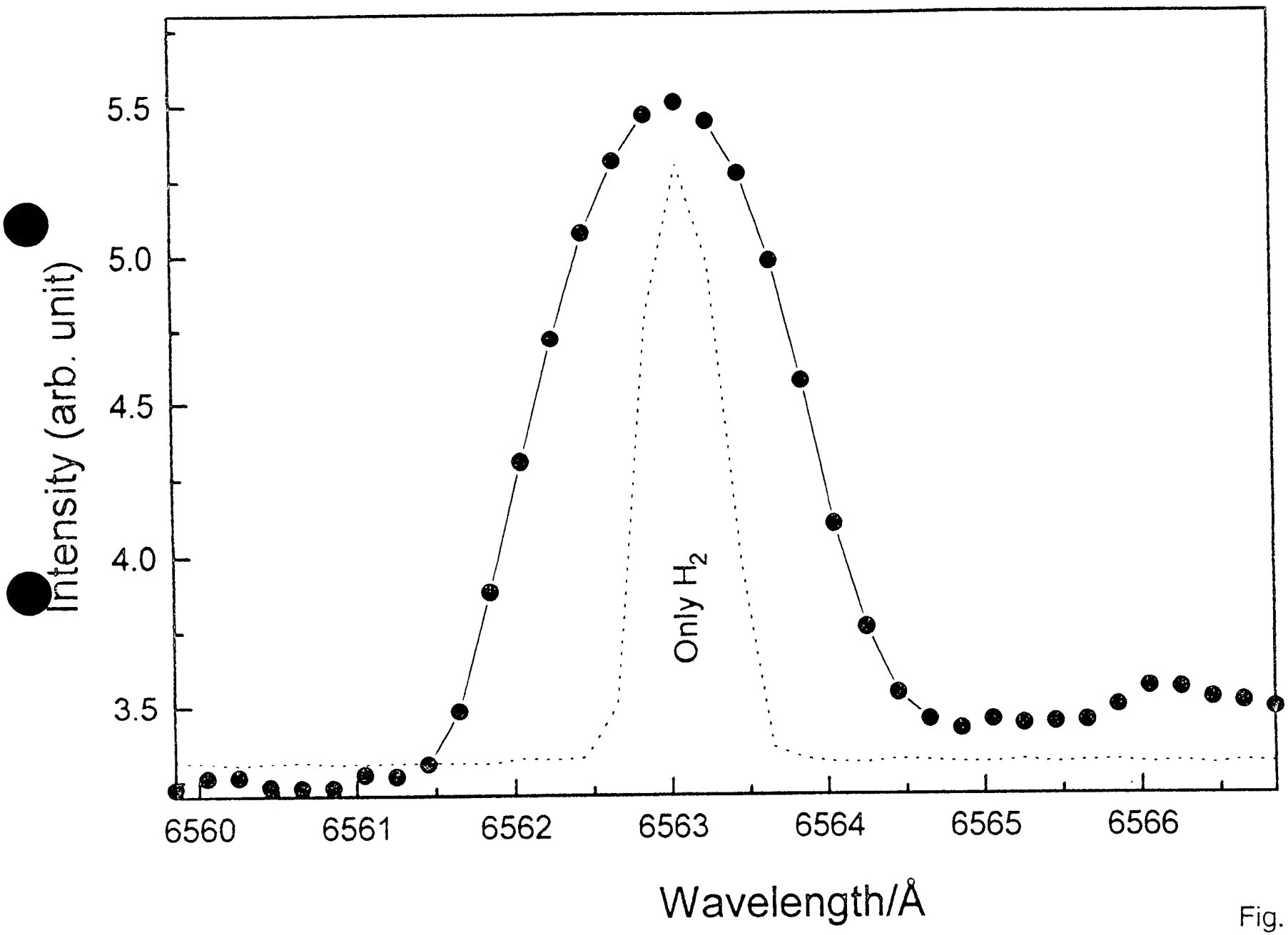
Intensity (arb. unit)
5.5
5.0
4.5
4.0
3.5
Only H_2
6560
6561
6562
6563
6564
6565
6566
Wavelength/Å

Fig. 4

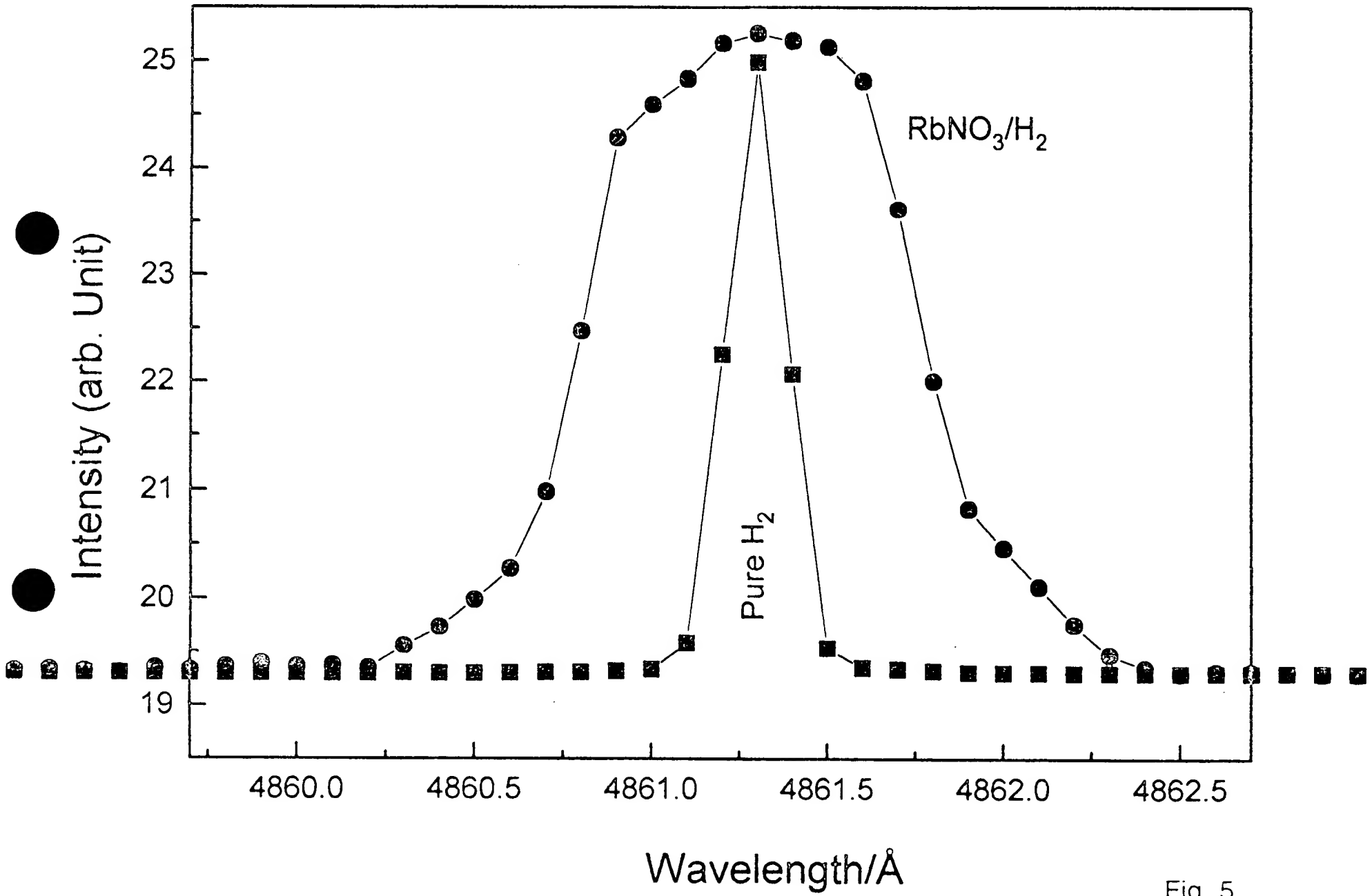
Intensity (arb. Unit)
25
24
23
22
21
20
19
RbNO3/H2
Pure H2
4860.0
4860.5
4861.0
4861.5
4862.0
4862.5
Wavelength/Å

Fig. 5

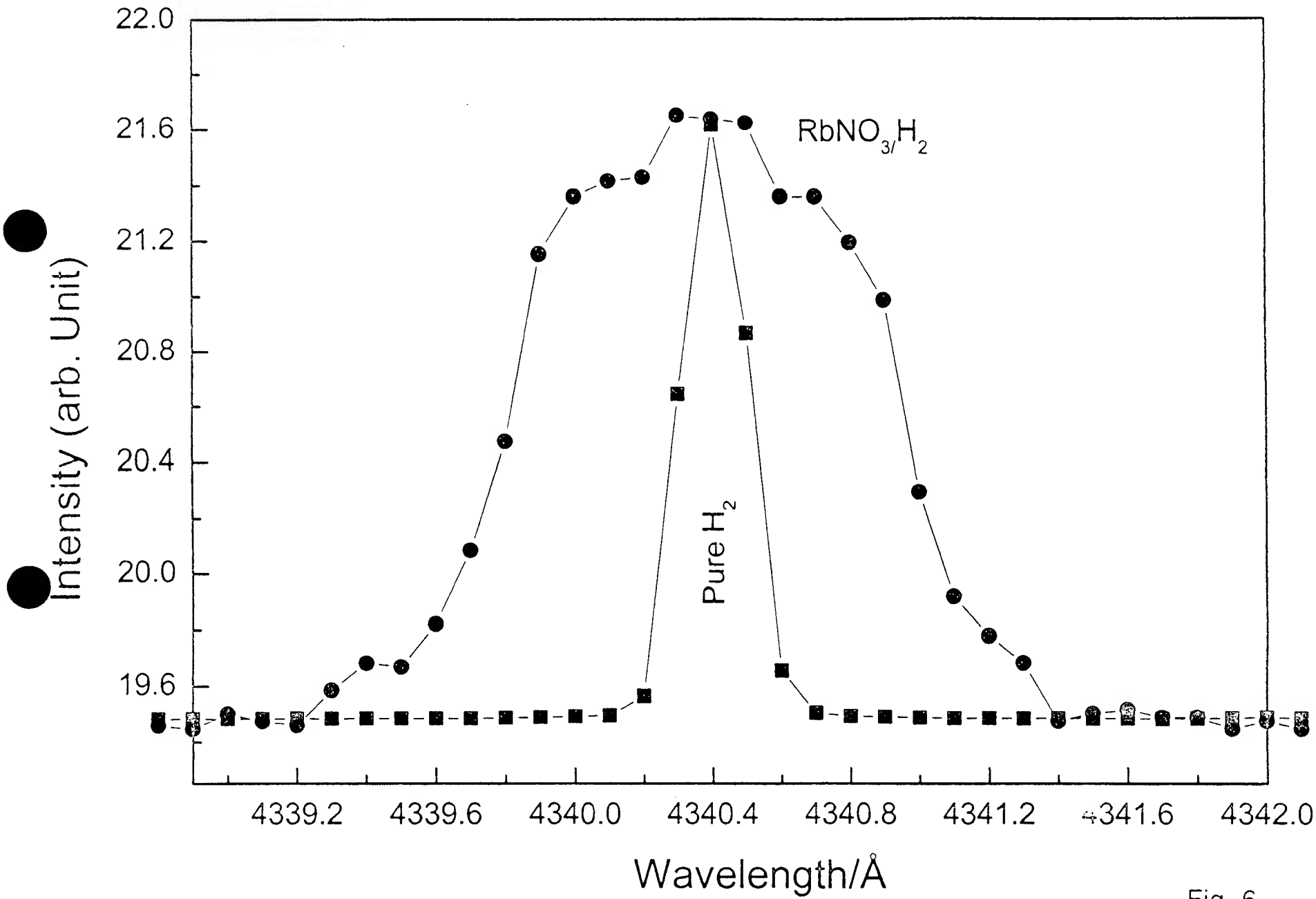
22.0
21.6
21.2
20.8
20.4
20.0
19.6
Intensity (arb. Unit)
RbNO3/H2
Pure H2
4339.2
4339.6
4340.0
4340.4
4340.8
4341.2
4341.6
4342.0
Wavelength/Å

Fig. 6

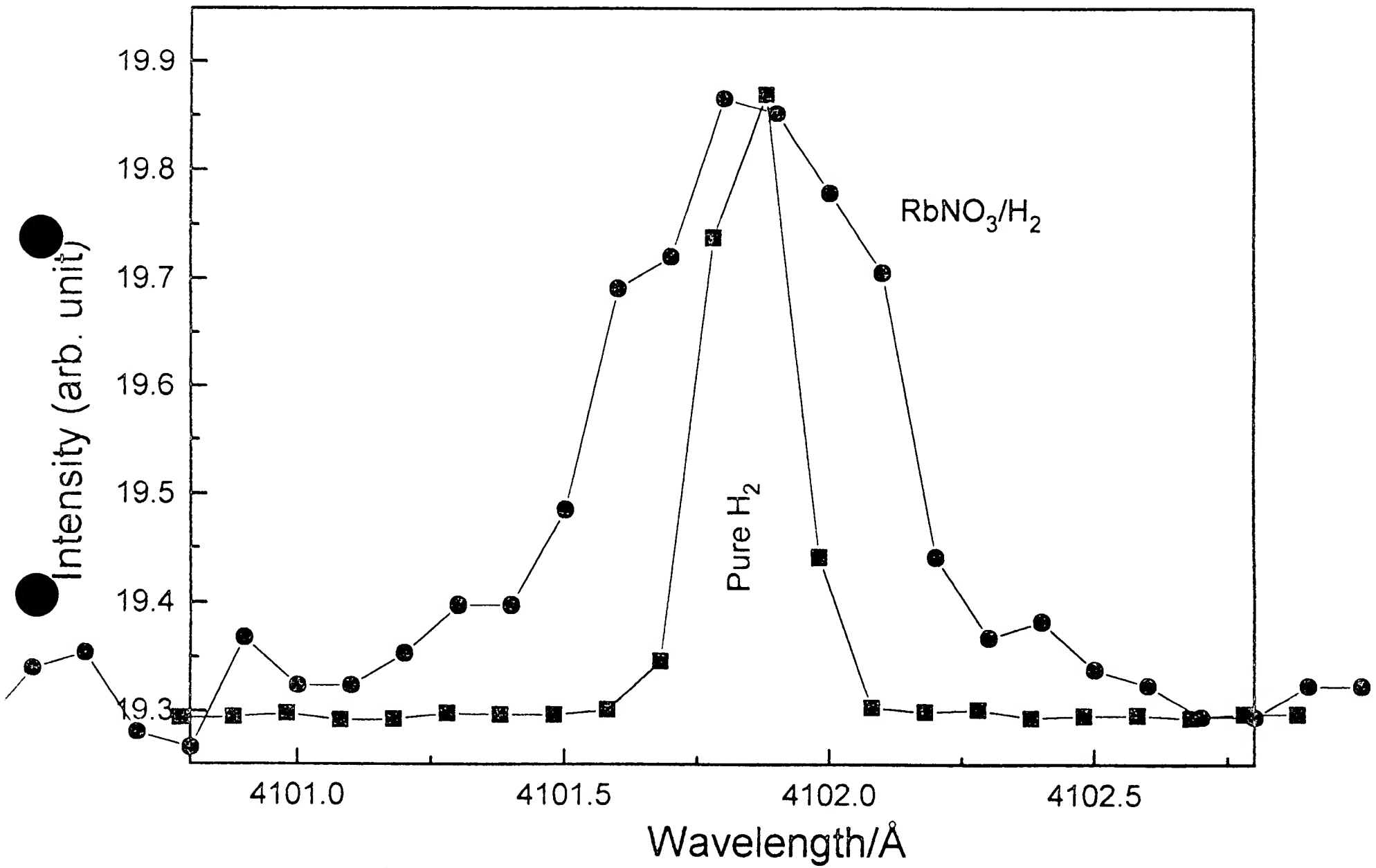
19.9
19.8
19.7
19.6
19.5
19.4
19.3
Intensity (arb. unit)
RbNO3/H2
Pure H2
4101.0
4101.5
4102.0
4102.5
Wavelength/Å

Fig. 7

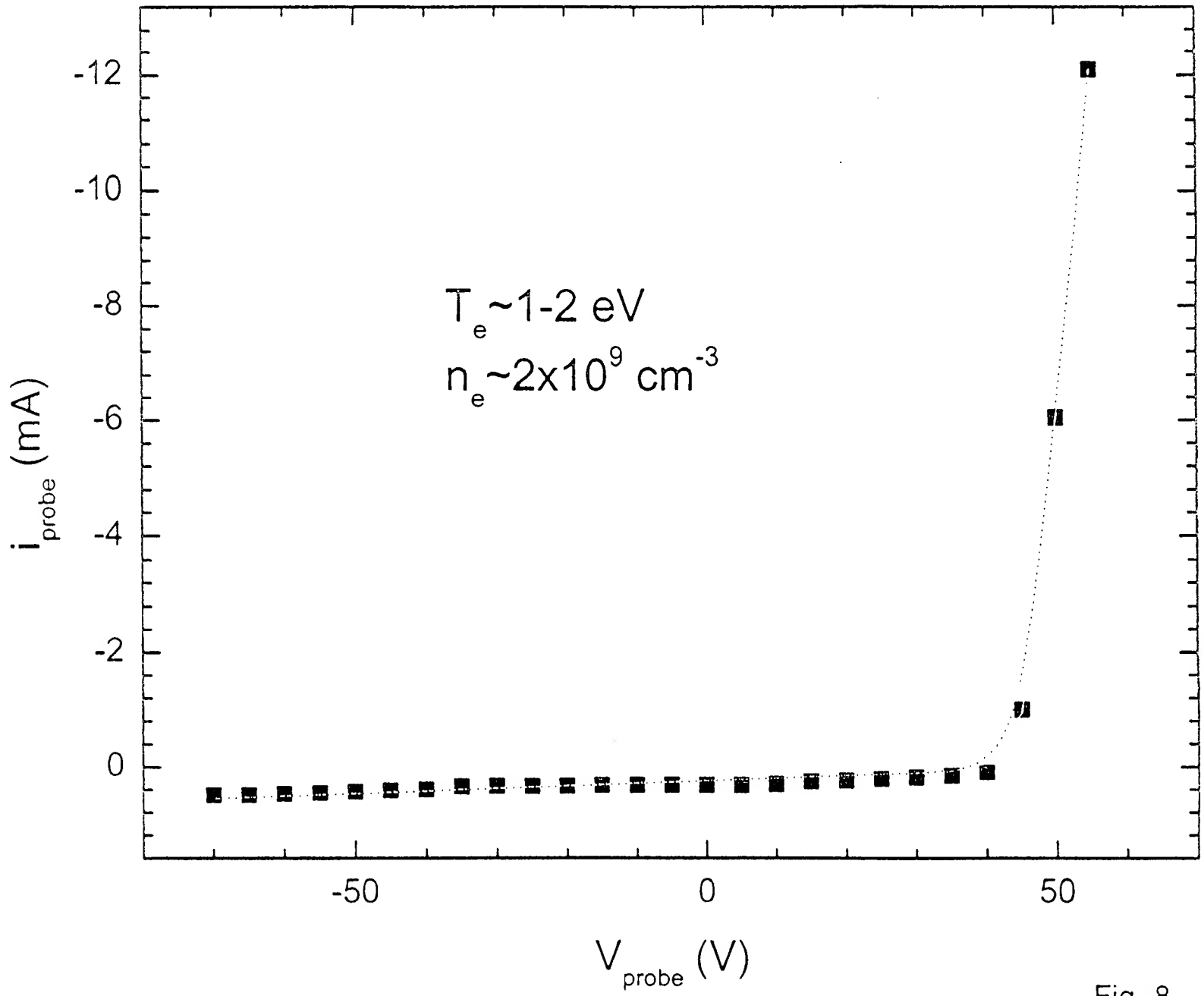

Fig. 8

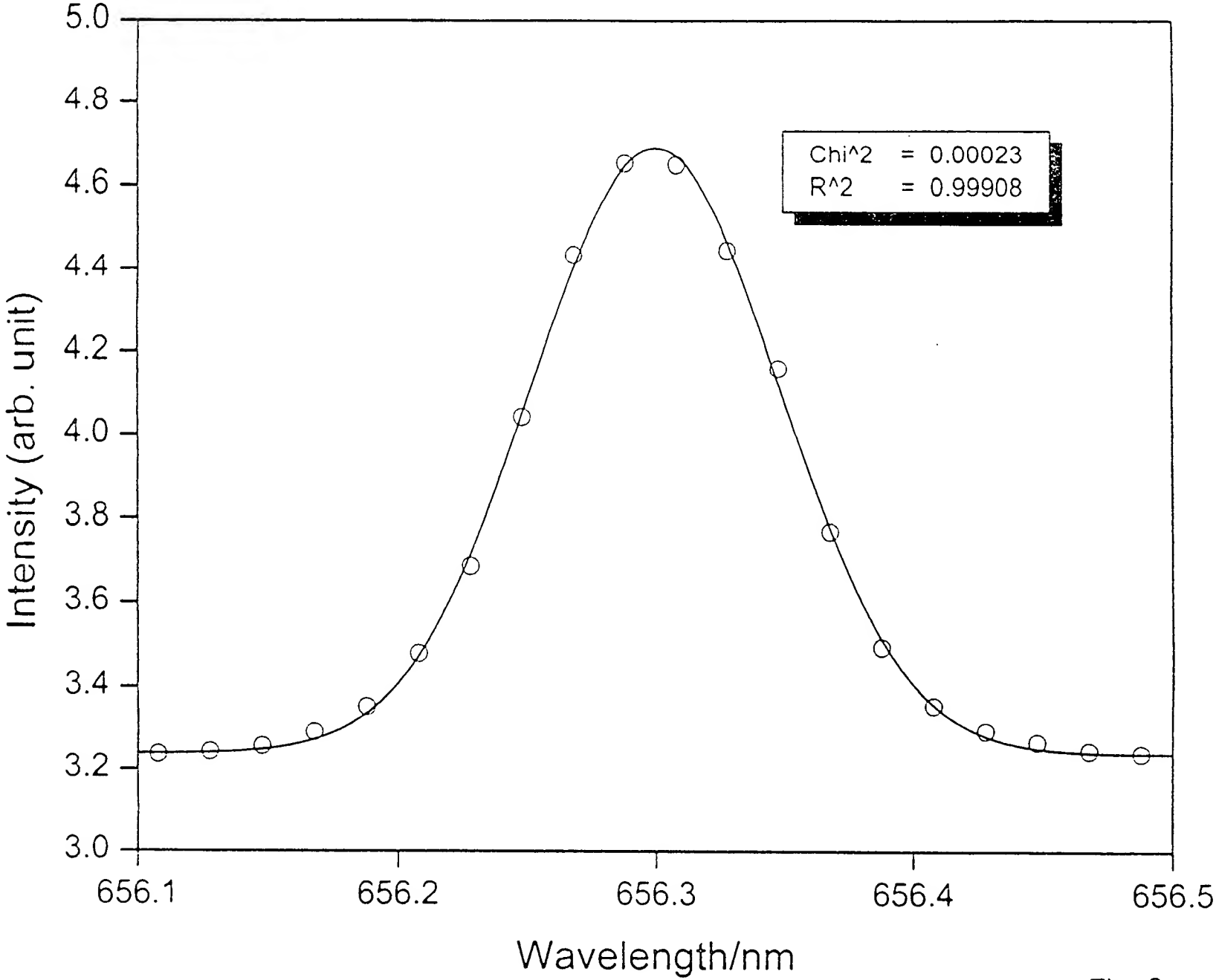
Chi^2 = 0.00023
R^2 = 0.99908
Intensity (arb. unit)
5.0
4.8
4.6
4.4
4.2
4.0
3.8
3.6
3.4
3.2
3.0
656.1
656.2
656.3
656.4
656.5
Wavelength/nm

Fig. 9

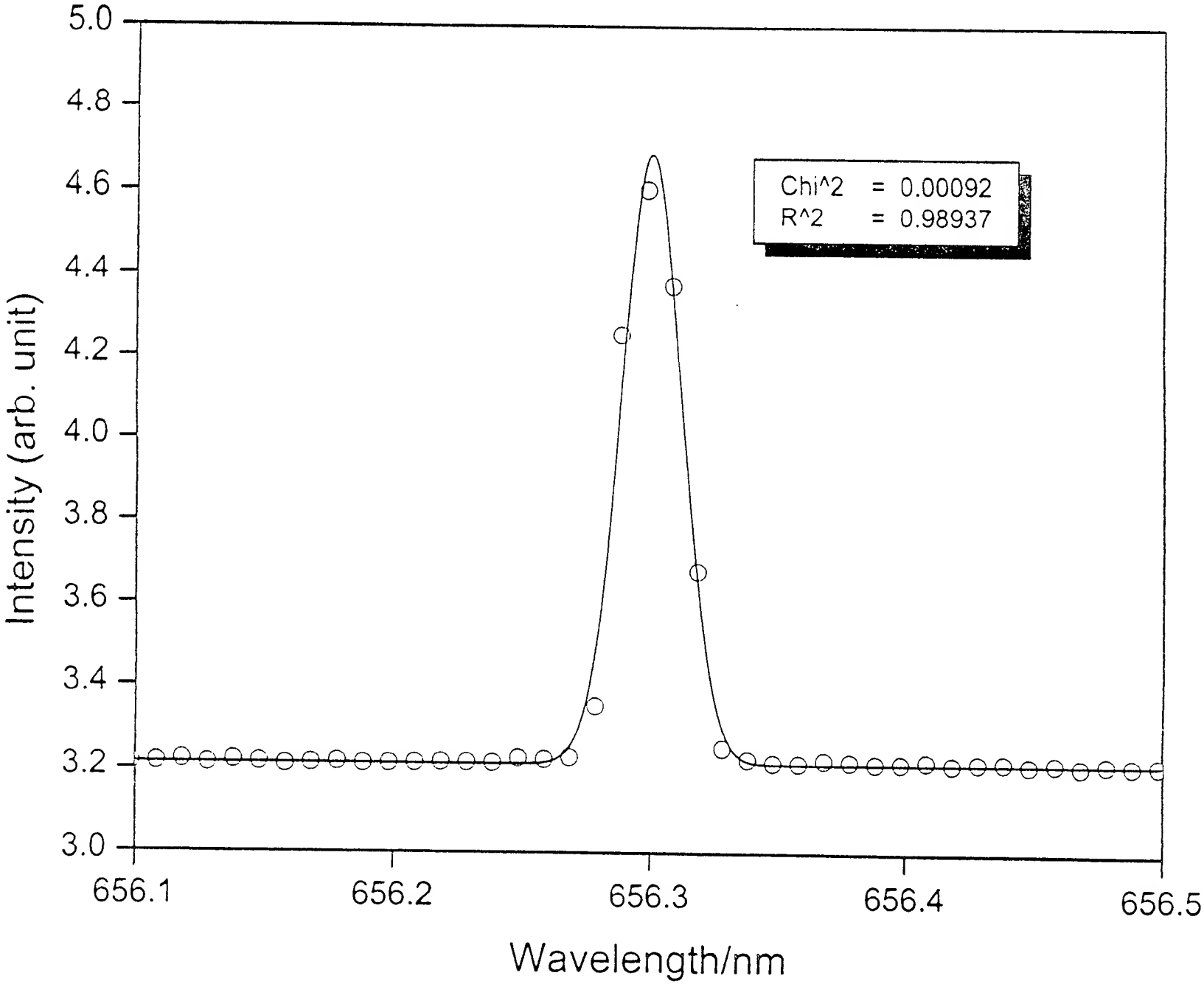
5.0
4.8
4.6
4.4
4.2
4.0
3.8
3.6
3.4
3.2
3.0
Intensity (arb. unit)
Chi^2 = 0.00092
R^2 = 0.98937
656.1
656.2
656.3
656.4
656.5
Wavelength/nm

Fig. 10

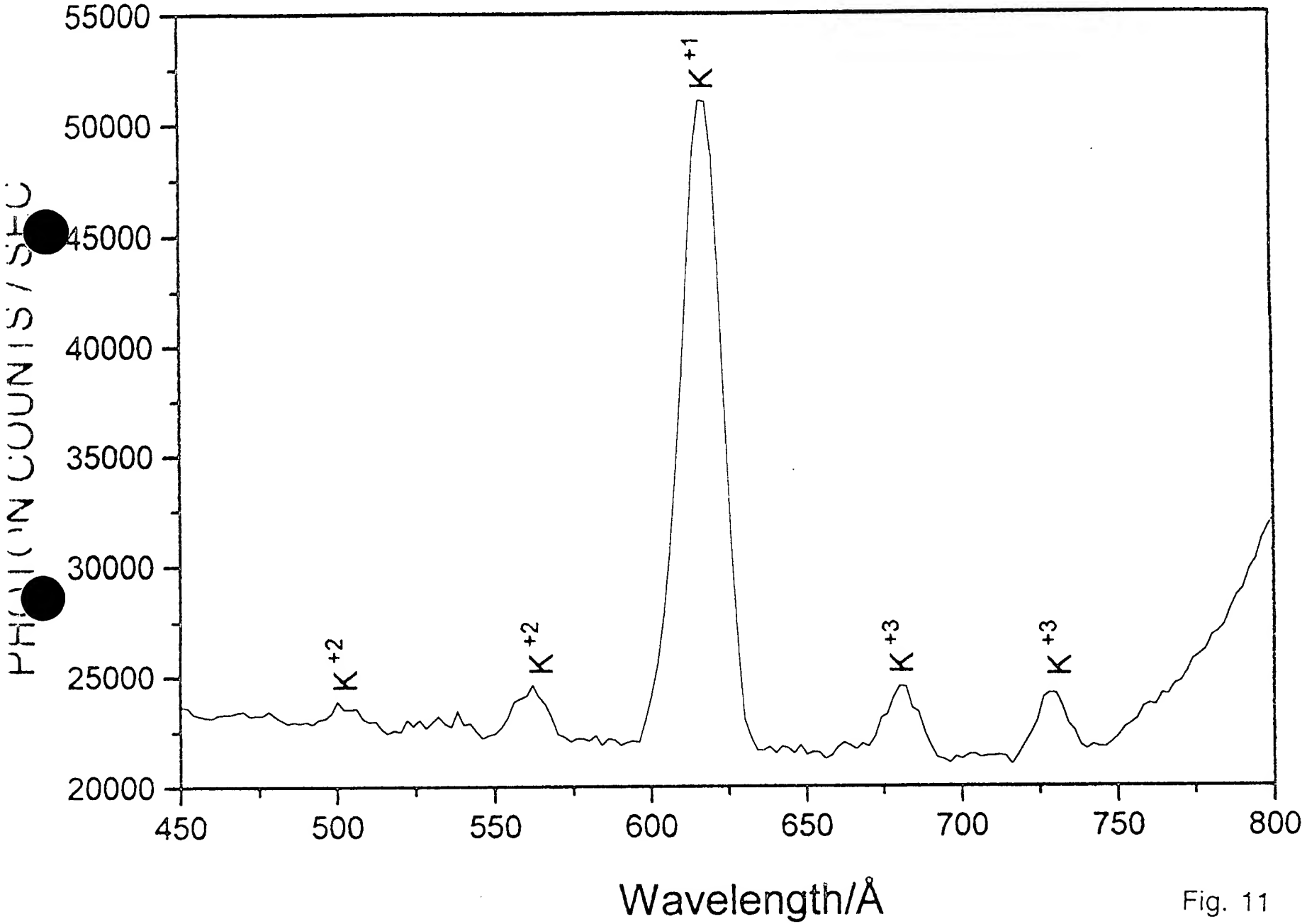
55000
50000
45000
40000
35000
30000
25000
20000
PHOTON COUNTS / SEC
450
500
550
600
650
700
750
800
Wavelength/Å
K+2
K+2
K+1
K+3
K+3

Fig. 11

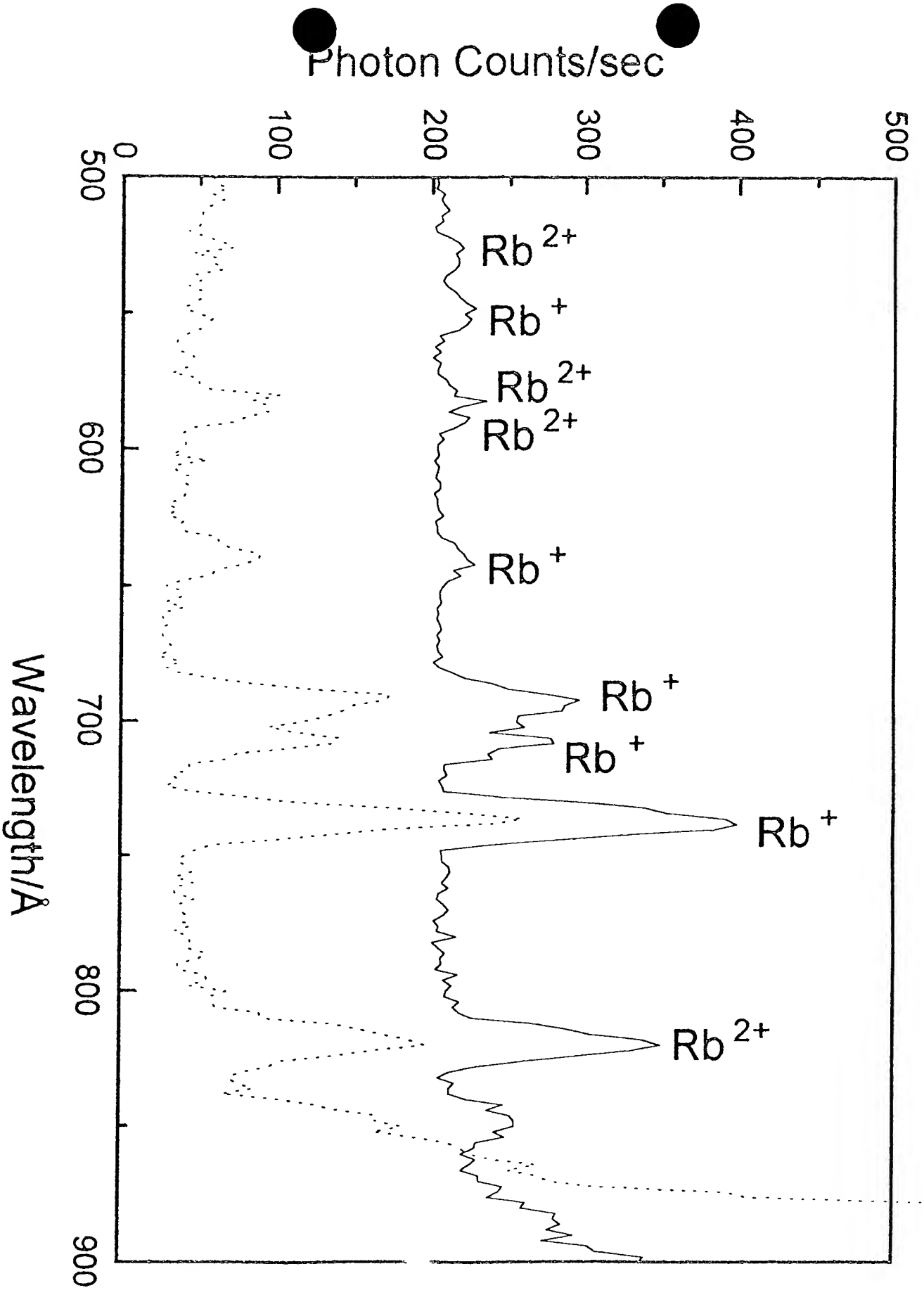
Photon Counts/sec
0
100
200
300
400
500
Wavelength/Å
500
600
700
800
900
Rb 2+
Rb +
Rb 2+
Rb 2+
Rb +
Rb +
Rb +
Rb +
Rb 2+

Fig. 12

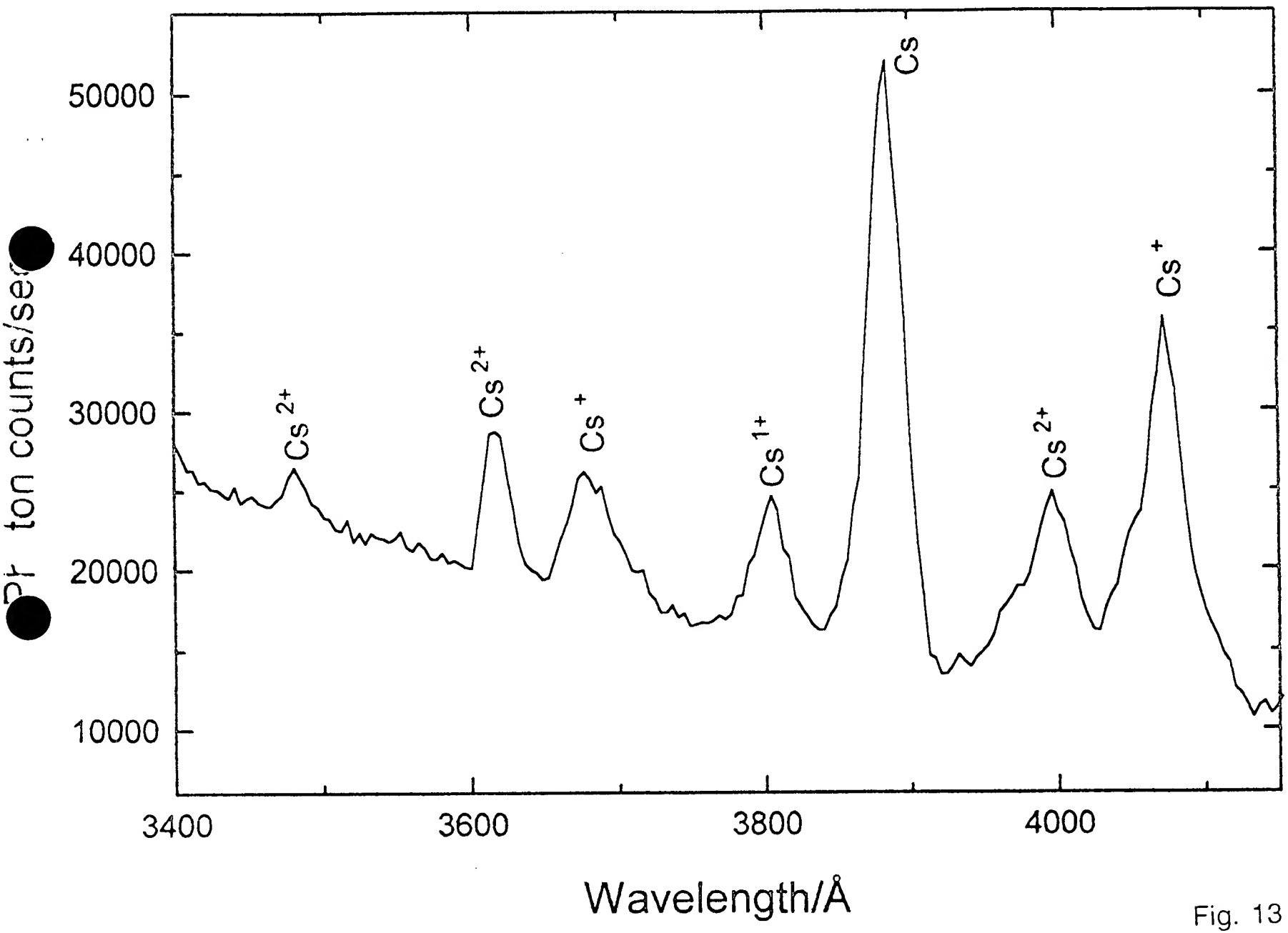
50000
40000
30000
20000
10000
3400
3600
3800
4000
Wavelength/Å
Cs
Cs 2+
Cs 2+
Cs +
Cs 1+
Cs 2+
Cs +

Fig. 13

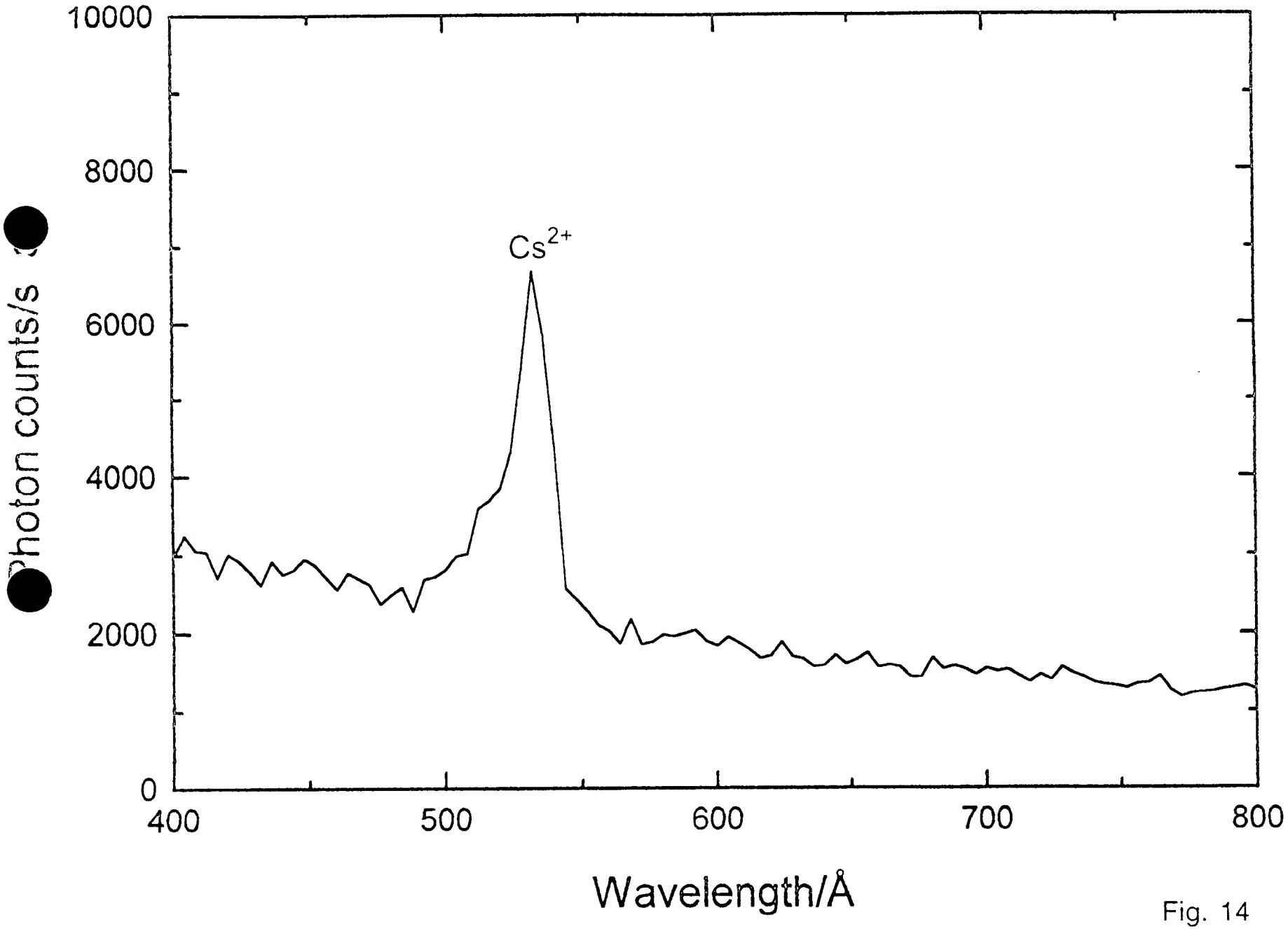
10000
8000
6000
4000
2000
0
Photon counts/s
Cs2+
400
500
600
700
800
Wavelength/Å

Fig. 14

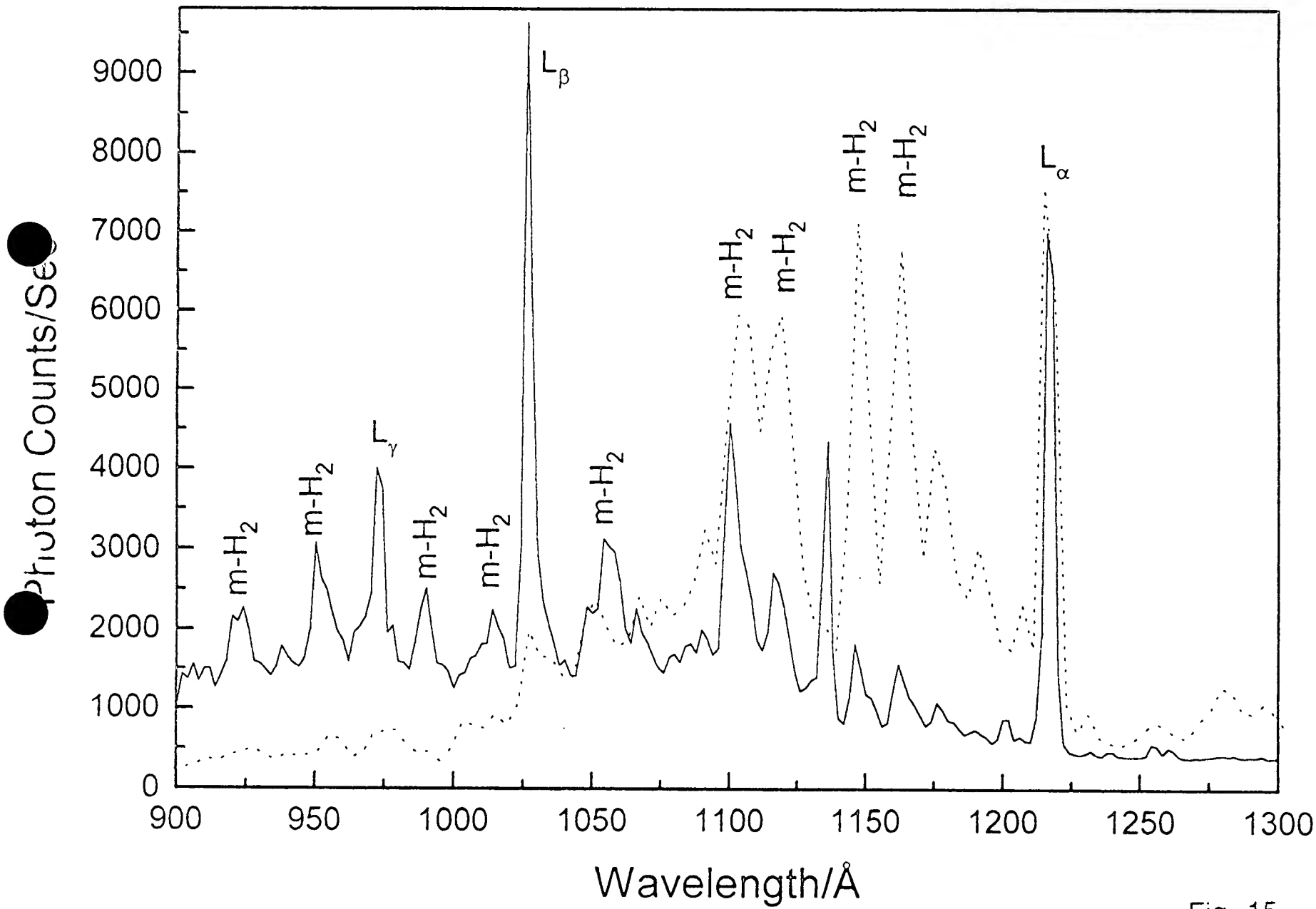
Photon Counts/Sec
9000
8000
7000
6000
5000
4000
3000
2000
1000
0
900
950
1000
1050
1100
1150
1200
1250
1300
Wavelength/Å
m-H2
Γγ
Γβ
Γα

Fig. 15

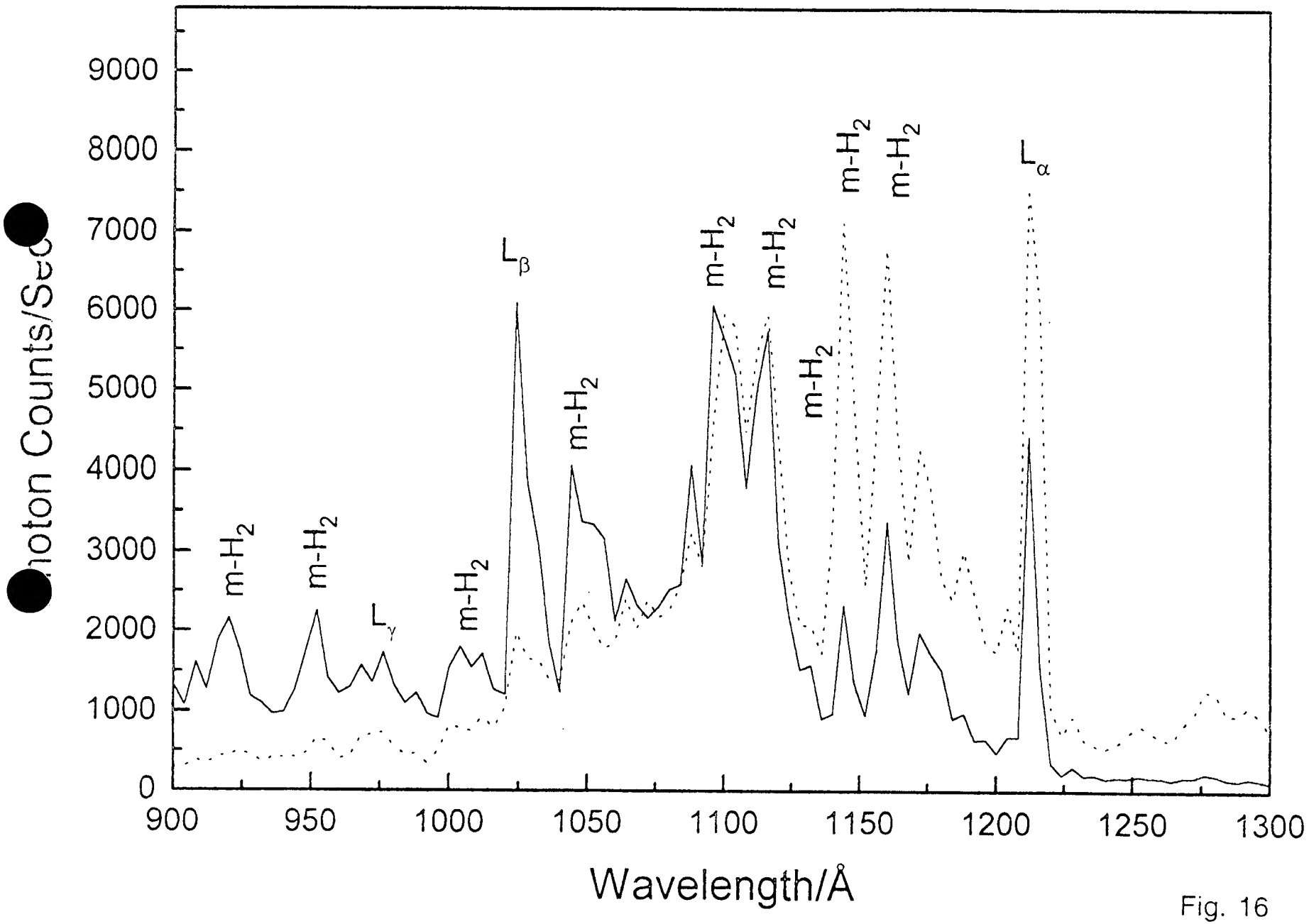
9000
8000
7000
6000
5000
4000
3000
2000
1000
0
900
950
1000
1050
1100
1150
1200
1250
1300
Wavelength/Å
m-H2
m-H2
Lγ
m-H2
Lβ
m-H2
m-H2
m-H2
m-H2
m-H2
Lα

Fig. 16

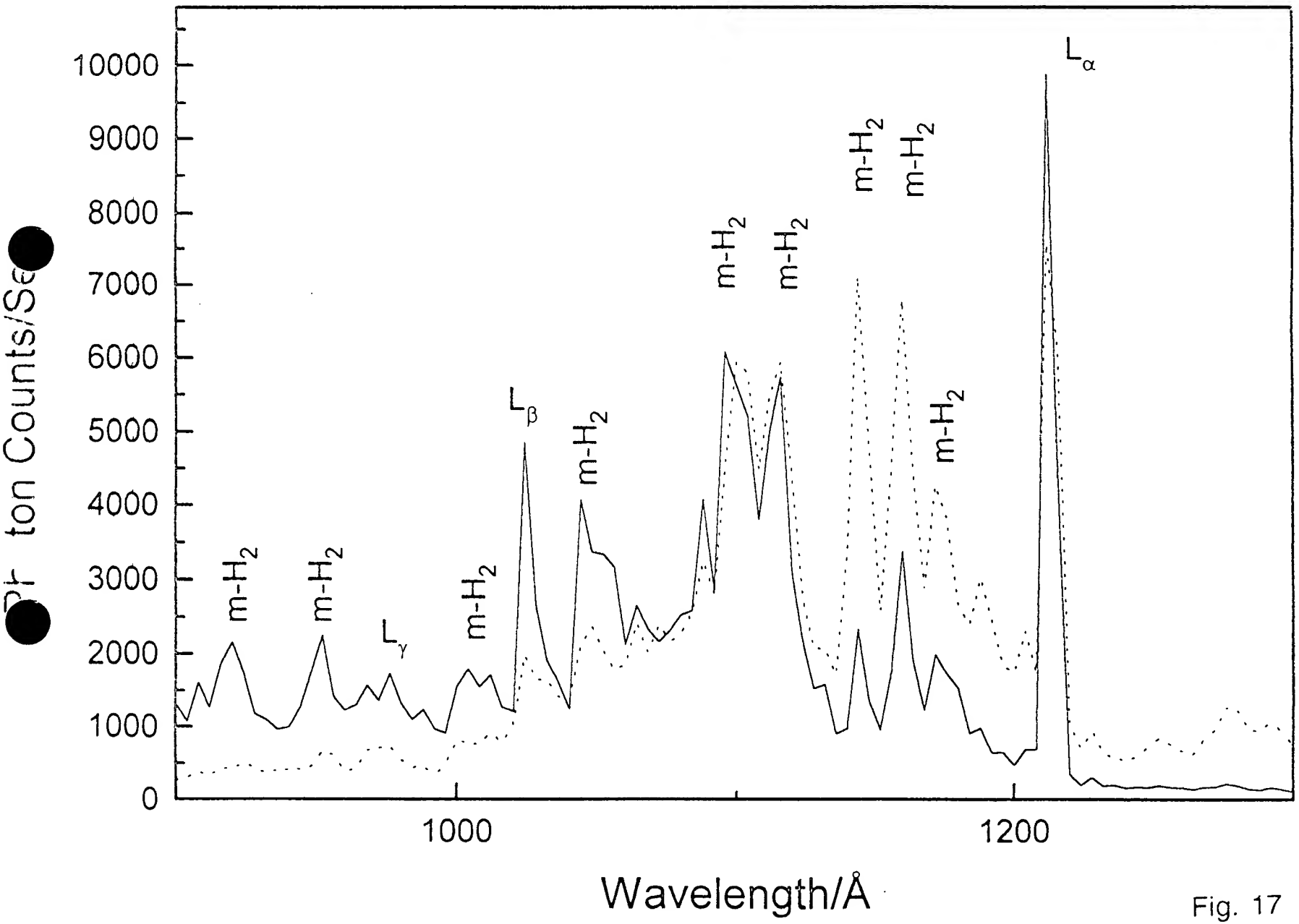
10000
9000
8000
7000
6000
5000
4000
3000
2000
1000
0
1000
1200
Wavelength/Å
m-H2
m-H2
Lγ
m-H2
Lβ
m-H2
m-H2
m-H2
m-H2
m-H2
Lα

Fig. 17

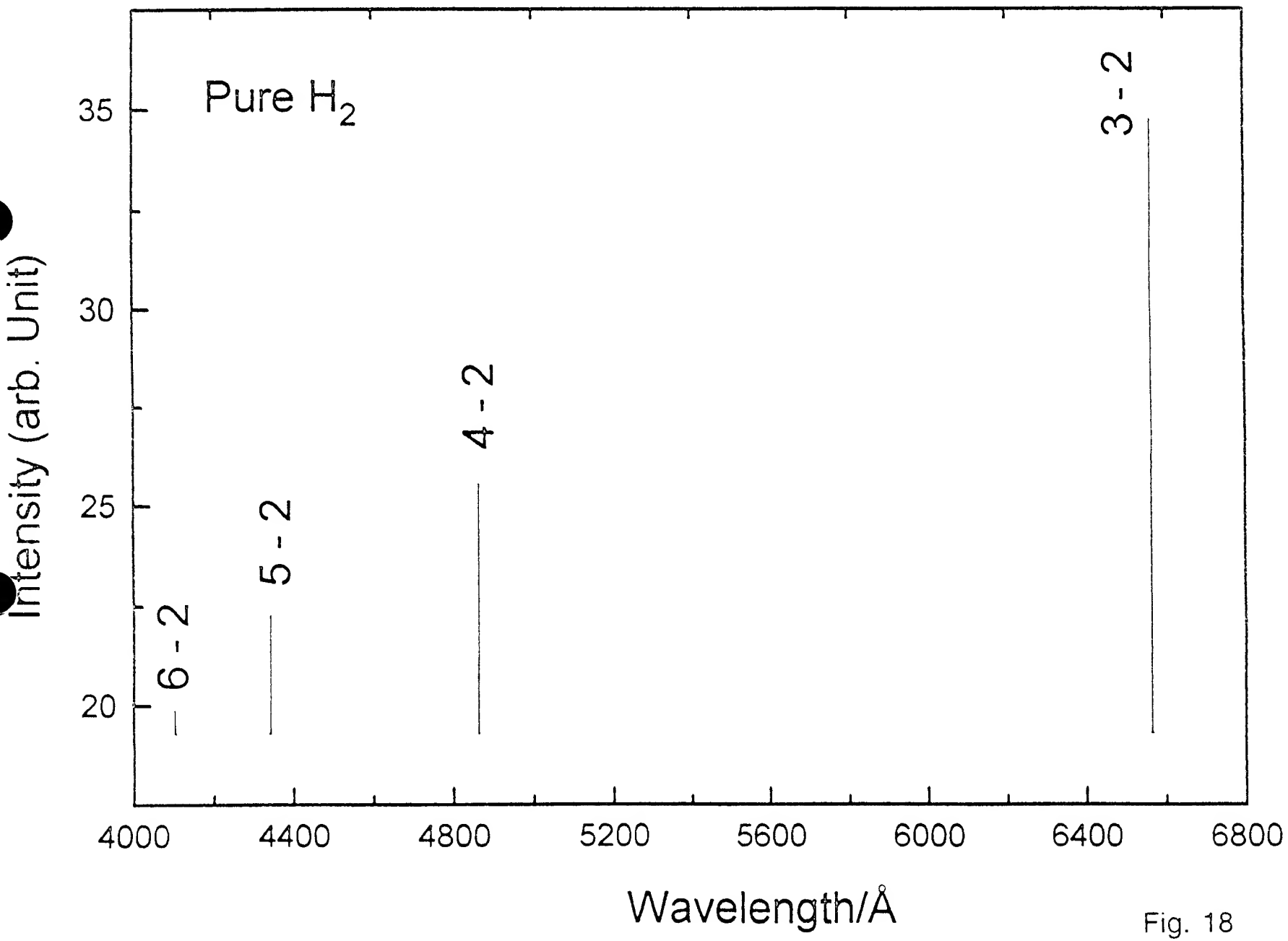
Pure H_2
Intensity (arb. Unit)
35
30
25
20
6 - 2
5 - 2
4 - 2
3 - 2
4000
4400
4800
5200
5600
6000
6400
6800
Wavelength/Å

Fig. 18

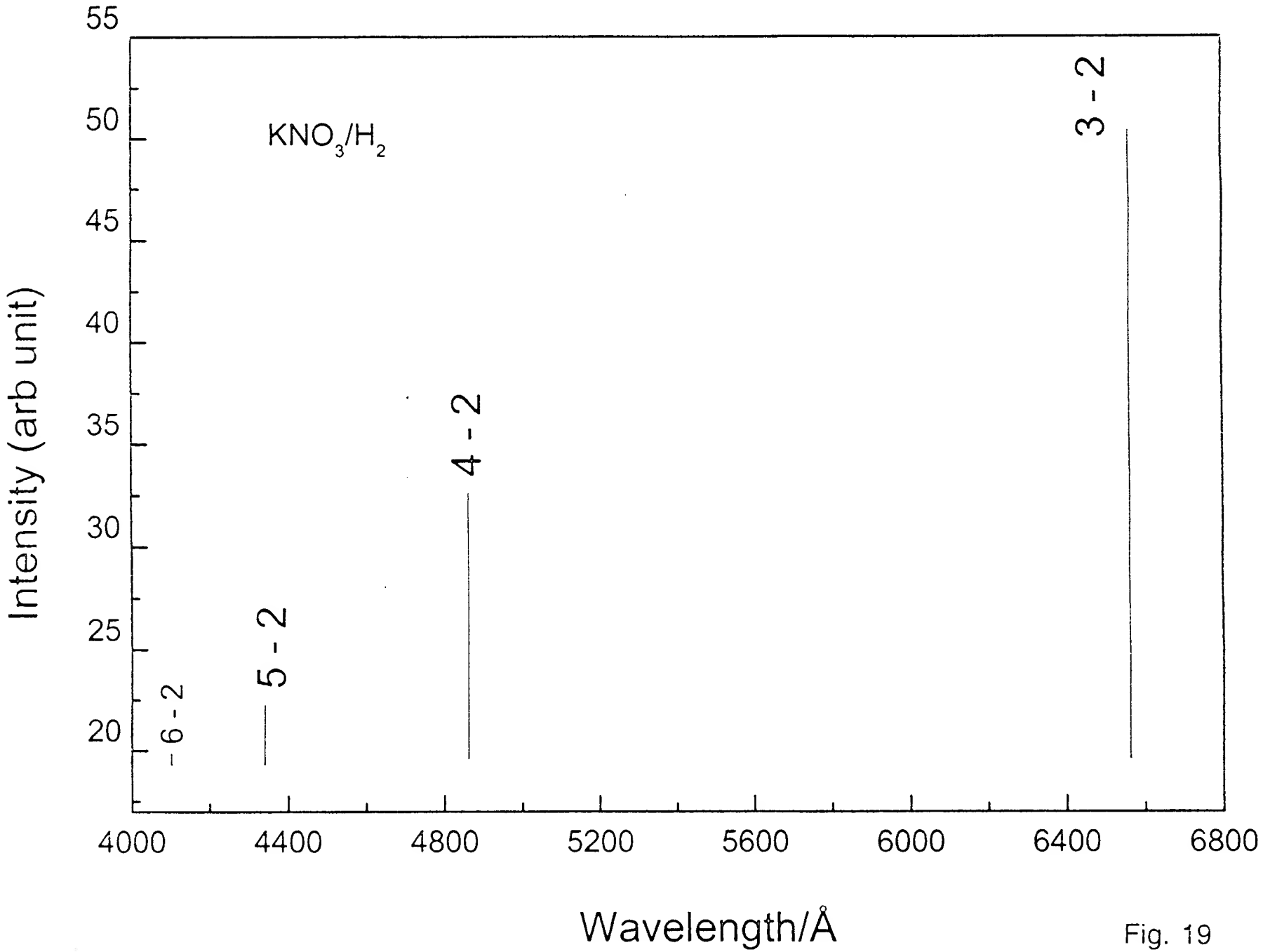
55
50
45
40
35
30
25
20
Intensity (arb unit)
KNO3/H2
3 - 2
4 - 2
5 - 2
6 - 2
4000
4400
4800
5200
5600
6000
6400
6800
Wavelength/Å

Fig. 19

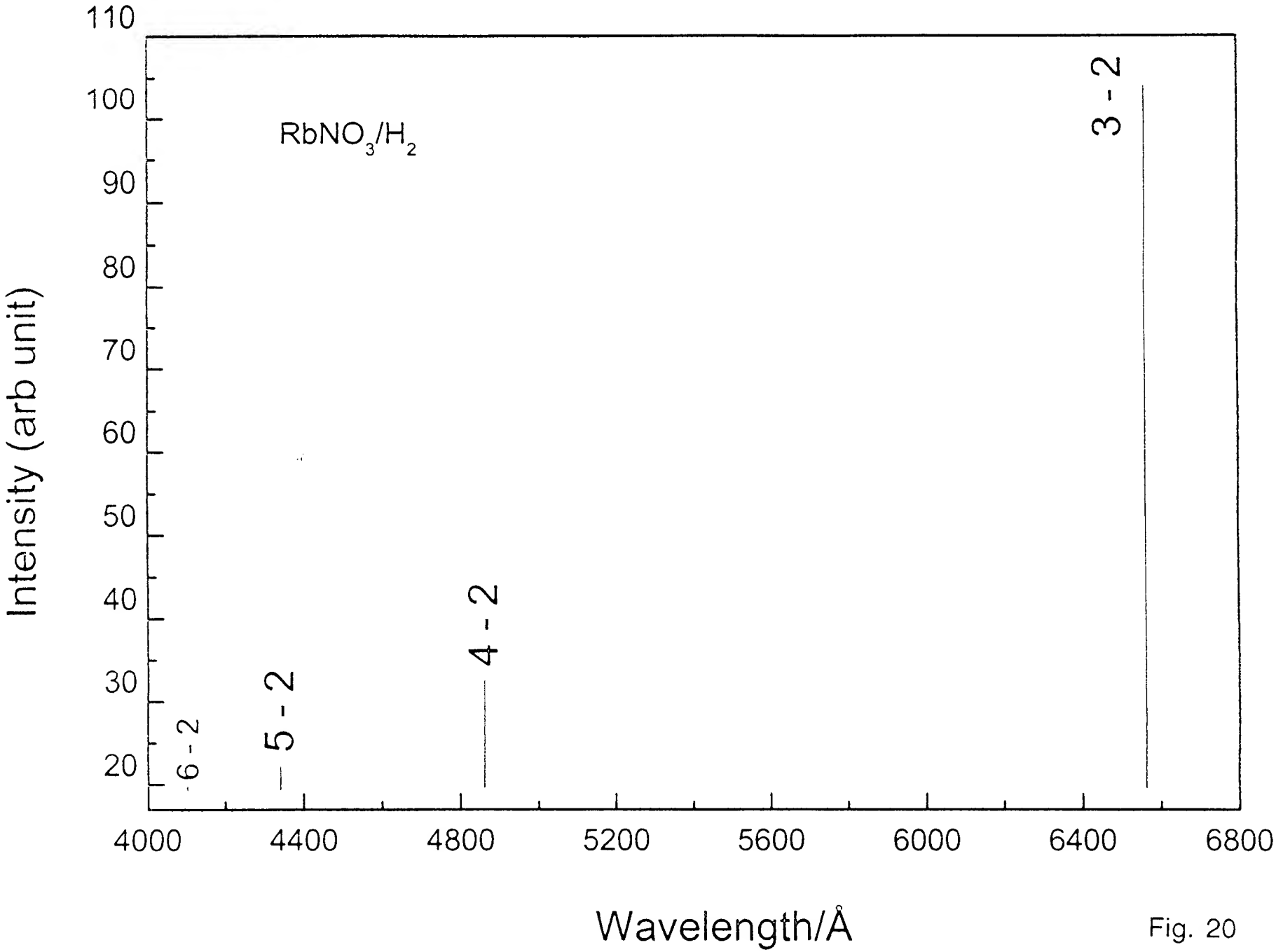
110
100
90
80
70
60
50
40
30
20
Intensity (arb unit)
RbNO3/H2
3 - 2
4 - 2
5 - 2
6 - 2
4000
4400
4800
5200
5600
6000
6400
6800
Wavelength/Å

Fig. 20

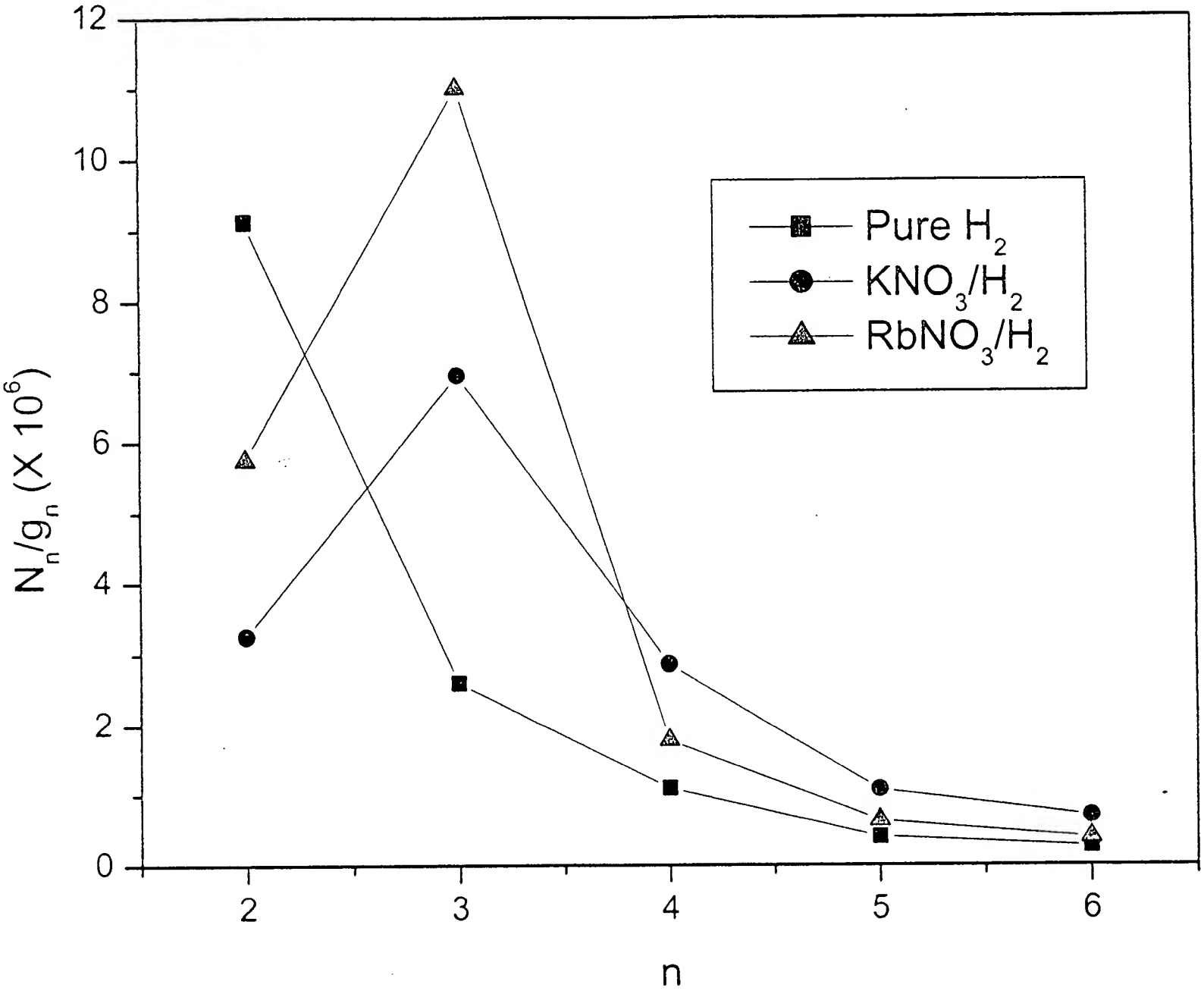

Fig. 21